1 **Title:** CD226 identifies effector CD8^{+} T cells during tuberculosis and costimulates recognition of

2 *Mycobacterium tuberculosis*-infected macrophages

3

4 **Authors:** Tomoyo Shinkawa[1], Evelyn Chang[1,2], Tasfia Rakib[1,2], Kelly Cavallo[1], Rocky Lai[1], and

5 Samuel M. Behar[1*]

6

7 **Affiliations**:

8 1. Department of Microbiology, University of Massachusetts Medical School,

9 Worcester, Massachusetts, USA.

10 2. Immunology and Microbiology Program, Graduate School of Biomedical Science, Worcester,

11 Massachusetts, USA.

12

13 *Corresponding author

14 Samuel M. Behar

15 E-mail address: samuel.behar@umassmed.edu (SMB)

16

Abstract: CD8^{+} T cells defend against *Mycobacterium tuberculosis* (Mtb) infection but variably recognize Mtb-infected macrophages. To define how the diversity of lung parenchymal CD8^{+} T cells changes during chronic infection, cells from C57BL/6J mice infected for 6- and 41-weeks were analyzed by scRNA-seq. We identified an effector lineage, including a cluster that expresses high levels of cytotoxic effectors and cytokines, and dysfunctional lineage that transcriptionally resembles exhausted T cells. The most significant differentially expressed gene between two distinct CD8^{+} T cell lineages is CD226. Mtb-infected IFNγ-eYFP reporter mice revealed IFNγ production is enriched in CD226^{+}CD8^{+} T cells, confirming these as functional T cells in vivo. Purified CD226^{+} but not CD226^{−} CD8^{+} T cells recognize Mtb-infected macrophages, and CD226 blockade inhibits IFNγ and granzyme B production. Thus, CD226 costimulation is required for efficient CD8^{+} T cell recognition of Mtb-infected macrophages, and its expression identifies CD8^{+} T cells that recognize Mtb-infected macrophages.

One Sentence Summary: Shinkawa et al. discover that CD226 is a functional marker that distinguishes effector from dysfunctional CD8^{+} T cells in the *Mycobacterium tuberculosis* (Mtb)-infected lung and has a crucial role in costimulating CD8^{+} T cell recognition of Mtb-infected macrophages.

Main Text:

Introduction

Mycobacterium tuberculosis (Mtb), the bacterium that causes the human disease tuberculosis (TB), is an extraordinarily successful intracellular pathogen that coevolved with humans and developed ways to evade our host defenses. It is estimated that Mtb has infected 25% of the world's population (*1*). Only 5-10% of infected people develop TB, which attests to the effectiveness of human immunity. Mtb-specific T cells are essential to prevent TB in humans and control infection in animal models (*2-4*). Mtb elicits strong CD8^{+} T cell responses associated with Mtb control in humans and experimentally infected animals (*4-16*). In the mouse TB model, polyclonal CD8^{+} T cells elicited by infection can restrict Mtb in vitro (*17*) and in vivo (*13*), and vaccine-elicited CD8^{+} T cell responses improve control of pulmonary TB (*18, 19*). CD8^{+} T cells are essential for the long-term survival of mice following intravenous Mtb infection (*12, 20*). These data show the potential of CD8^{+} T cell responses to combat Mtb infection. However, CD8^{+} T cell depletion leads to only modest reductions in survival after low-dose aerosol infection (*4*). Thus, the mechanisms of how CD8^{+} T cells mediate immunity, and how Mtb evades effective CD8^{+} T cell responses are poorly understood.

A priori, three scenarios could limit immunity mediated by CD8^{+} T cells. First, Mtb could have evolved to avoid CD8^{+} T cell recognition by producing decoy antigens or avoiding antigen entry into the class I MHC pathway. We described the inefficient presentation of the immunodominant TB10.4 antigen by Mtb-infected macrophages to CD8^{+} T cells (*21-23*) and found that only 10-15% of CD8^{+} T cells from the lungs of Mtb-infected C57BL/6J mice recognize infected macrophages (*24*). Second, CD8^{+} T cells might fail to express effector functions associated with Mtb control. Among human T cells, tri-cytotoxic cells that express perforin, granzymes and granulysin are associated with anti-mycobacterial activity (*7, 8, 10*). While the absence of a granulysin ortholog in the *Mus* genome could explain why mice are unable to clear Mtb, a suitable model to test this hypothesis is not currently available (*25*). Finally, Mtb-specific CD8^{+} T cells

might become dysfunctional because of persistent stimulation, as has been observed during chronic viral infection and cancer. Continued T cell stimulation by persistent antigen induces a CD8^{+} T cell state known as exhaustion (*26, 27*). Exhausted CD8^{+} T cells have sustained expression of inhibitory receptors, reduced effector function, and diminished proliferation. Sustained inhibitory receptor expression, including PD-1 and TIM-3, on a subset of CD8^{+} T cells occurs in the murine TB model when the immune system is perturbed (*17, 28*) and in chronically infected mice (*29*). However, the underlying heterogeneity in phenotype and functionality of CD8^{+} T cells throughout infection is ill-defined. Whether T cell exhaustion occurs in human and non-human primates is also less clear (*30-32*).

To investigate the factors that compromise CD8^{+} T cell immunity, we used scRNA-seq and paired scTCR-Seq to define the heterogeneity of lung parenchymal CD8^{+} T cell responses during Mtb infection, early after the establishment of T cell-mediated control in infected C57BL/6J mice (i.e., 6 weeks post-infection, wpi) and during chronic infection (i.e., 41 wpi). CD8^{+} T cell responses are diverse and evolve over time. We find two major lineages of differentiation. One is an effector lineage, including a cluster of polyfunctional effectors; the other is a dysfunctional lineage that are transcriptionally similar to exhausted CD8^{+} T cells described during chronic LCMV infection and cancer. Dysfunctional CD8^{+} T cells increase in proportion over time. Notably, the gene encoding CD226 (DNAX accessory molecule-1; DNAM-1) is the most significantly differentially expressed gene (DEG) between effector and dysfunctional CD8^{+} T cell lineages. CD226 was first discovered as an adhesion molecule that enhances cytotoxicity in NK and T cells (*33*). Recent studies show that CD226 expression by CD8^{+} T cells is a favorable prognostic factor for cancer outcomes in humans and mice, and the efficacy of immune checkpoint blockade requires CD226 expression on CD8^{+} T cells (*34-37*). Using flow cytometry, IFNγ reporter mice, and an in vitro Mtb infection model, we show that CD226 is a marker that identifies effector CD8^{+} T cells with retained polyfunctionality, which persists during chronic infection in vivo. In vitro, not only does CD226 identify CD8^{+} T cells that recognize Mtb-infected macrophages, but blocking

87   CD226 impairs the production of effector molecules, including IFNγ and granzyme B by CD8^{+} T

88   cells, suggesting that CD226 is required for efficient recognition of infected macrophages.

89   Dysfunctional CD8^{+} T cells, characterized by a lack of CD226 expression and inability to recognize

90   infected macrophages, emerge as early as 4 wpi and increase massively in proportion over time.

91   Our data provide novel mechanistic insights into effective CD8^{+} T cell immune response and its

92   failure during Mtb infection.

RESULTS

Nine CD8+ T cell states are identified after Mtb infection

To assess the heterogeneity of CD8+ T cells both early and late during chronic Mtb infection, we generated single cell (sc) RNA-seq and TCR-seq datasets of lung parenchymal (CD45-IV−) CD3+ T cells, 6- and 41-weeks post-infection (wpi) (Fig.S1A). After quality control, cells expressing both *CD8a* and *CD8b1* were selected for analysis (n=9,870). To avoid T cell receptor (TCR) genes influencing clustering, we removed TCR genes before scaling and dimensionality reduction (*38*). Unsupervised clustering identified nine clusters of CD8+ T cells (Fig.1A, B, Table S1). Cluster designations were based on immunological signatures and key differentially expressed genes (Fig.1C, D, Table S1).

Cluster 0 is designated as effector-like T cells (hereafter referred to as 'TEFF/0') based on the expression of *Klrg1*, *Cd226*, *Id2, Rora,* and *Ifng*. A large percentage of cells are TEFF/0, even at 41 wpi. CD8+ T cells in Cluster 1 express high levels of co-inhibitory receptors *Pdcd1*, *Tigit*, *Lag3,* and *Gzmk* and transcription factors (TFs) associated with T cell exhaustion (*Tox* and *Eomes*) (Fig.1A, C, D, Table S1). CD8+ T cells in Cluster 1 have also lower expression of adhesion and costimulatory molecules, including *Cd226* and *Jaml*, and cytokines, including *Ifng* and *Tnf*. Therefore, Cluster 1 is defined as exhausted (TEXH/1) based on their similarity to exhausted CD8+ T cells during LCMV clone 13 infection and in tumors (*39*). Downregulation of *Il18r1* on TEXH/1 suggests they lose responsiveness to IL-18 (*40*). TEXH/1 is the largest population at 41 wpi (Fig.1B). CD8+ T cells in Cluster 2 express *Il7r*, *Tcf7*, *Il18r1*, and *Cxcr3*. These cells are designated as stem-like or memory CD8+ T cells (TSL-M/2) as they express few, if any, genes associated with effector function. The CD8+ T cells in Cluster 3 are designated as naïve (TN/3) based on their expression of *Ccr7*, *Sell, Lef1, Dapl1*, *and Tcf7* (Fig.1D, Table S1). Cluster 4 CD8+ T cells express the adhesion molecules *Itgae* (CD103) and *Itga1* (CD49a) consistent with tissue-resident memory T cells (TRM/4) (Fig.1A-D). Their expression of *Gzmb, Klrk1* (NKG2D), and *Klrd1* (CD94) indicates potential cytotoxic T cell (CTL) activity. Interestingly, expression of *Pdcd1, Tigit*, *and Lag3* in

119 T$_{RM}$/4 suggests persistent TCR stimulation (*41*). Enrichment of TGFβ signaling signature (*42*) in

120 T$_{RM}$/4 is consistent with TGFβ affecting differentiation and maintenance of T$_{RM}$ (*43-47*) and co-

121 inhibitory receptor expression (*48*) (Fig.S1B).

122 The remaining 25% of CD8$^+$ T cells are distributed among Clusters 5-8. Cluster 5 shares

123 features with activated CD8$^+$ T cells, including upregulation of components of AP-1 family TFs,

124 *Fosb*, and *Jun*. However, they express mitochondrial and nuclear genes, including *Malat1 (49)*

125 and had low recovery of paired TCRα and TCRβ transcripts, suggesting dying or low-quality cells.

126 Cluster 6 is designated as polyfunctional CD8$^+$ T cells (T$_{POLY}$/6) based on their high expression

127 of *Ifng, Tnf, Prf1*, *Gzmb, Ccl3, and Ccl4.* Expression of Nr4a family TFs and *Tnfrsf9* suggests

128 active TCR signaling. The expression of exhaustion-related genes, including *Havcr2, Lag3,* and

129 *Rgs16,* could indicate chronic TCR stimulation (*50*). Cluster 7 CD8$^+$ T cells are proliferating

130 (T$_{PROLIF}$/7) based on *Mki67, Top2a, Stmn1*, and *Ube2c* expression. Finally, CD8$^+$ T cells in Cluster

131 8 have a type I interferon (IFN I) signature (T$_{IFN}$/8) based on *Ifit1, Ifit3, Bst2, Isg15*, and *Isg20*

132 expression.

133 To explore TF regulon activity in each CD8$^+$ T cell state, we performed Single-cell

134 Regulatory Network Inference and Clustering (SCENIC) (*51*). We identified increased expression

135 of target genes and TF activity of Rorα and Klf6 in T$_{EFF}$/0 (Fig.S1C). T$_{EXH}$/1 displayed high Eomes

136 activity, consistent with Eomes promoting CD8$^+$ T cell exhaustion (*52*). TF activity of Irf1, -2, -7,

137 and -9, and Stat1 and -2, are enriched in T$_{IFN}$/8, consistent with IFN I responses (Fig.S1C). We

138 inferred cytokine signaling activity using Cytokine Signaling Analyzer (CytoSig) (Fig.S1D)(*53*). A

139 pronounced response to IL-18 is predicted for T$_{EFF}$/0 and T$_{SL-M}$/2, supporting their designation

140 as effector and memory-like CD8$^+$ T cells (*40*). T$_{IFN}$/8 is expected to have an elevated response

141 to interferons and to IL-27 which induces co-inhibitory gene programs (*54*).

142 To confirm the clusters' identity, we applied gene signatures from a dataset of CD8$^+$ T

143 cells induced by Lymphocytic Choriomeningitis Virus (LCMV) Clone 13 infection. The "Effector-

144 like signature" has the highest score in T$_{EFF}$/0 and the lowest score in T$_{EXH}$/1 and T$_N$/3

145 (Fig.1E)(*39*). The "Terminally exhausted signature" also from LCMV Clone 13 infection, has the

146 highest score in $T_{EXH}/1$ and $T_{IFN}/8$ and the lowest score in $T_N/3$ and $T_{PROLIF}/7$ (Fig.1F)(*39*). The

147 high "Terminally exhausted signature" score for $T_{IFN}/8$ supports IFN I driving CD8$^+$ T cell

148 dysfunction (*55, 56*). To further substantiate our cluster annotations, we performed a label transfer

149 of other dataset which include CD8$^+$ T cells from both acute and chronic LCMV infection to our

150 dataset (*57, 58*). Nearly all $T_{EFF}/0$ cells are identified as effector (T_{EFF}), a CD8$^+$ T cell state

151 observed exclusively after acute LCMV infection, but not chronic LCMV infection (Fig.1G,

152 Fig.S1E, F). CD8$^+$ T cells from chronic LCMV infection (e.g. "Exh−Int," "Exh−term," Fig.S1F)

153 project onto $T_{EXH}/1$ and $T_{RM}/4$, which increase in proportion at 41 wpi. This analysis confirms that

154 $T_{EFF}/0$ and $T_{POLY}/6$ are in effector states, while $T_{EXH}/1$ is in an exhausted state. $T_{RM}/4$ has a

155 mixed feature of effector and exhausted states. In summary, we identify nine distinct clusters of

156 CD8$^+$ T cells, present both early and late after Mtb infection, including clusters with multiple

157 effector molecule expression and clusters that resemble exhausted CD8$^+$ T cells.

158

159 **Cd226 distinguishes between effector-like and dysfunctional CD8$^+$ T cell lineages**

160 To understand lineage relationship of CD8$^+$ T cell clusters and to infer which responses

161 are driven by Mtb infection, we leveraged paired scTCR-seq analysis (Table S2). Clonal

162 expansions are a cardinal feature of T cell responses and cells with identical TCR rearrangements

163 indicate a common origin. T cells with identical CDR3α and CDR3β nucleotide sequences were

164 defined as a clonotype. We identified 1,187 unique TCRαβ clonotypes among 5,833 cells.

165 Dramatic expansions were detected in $T_{EFF}/0$ consistent with an effector CD8$^+$ T cell response to

166 Mtb infection (Fig.2A). In contrast, expansions of clonotypes in $T_{EXH}/1$ were smaller and most

167 clonotypes in $T_N/3$ were unique, consistent with their exhausted and naïve T cell designation,

168 respectively.

169 The Morisita index was used to quantify TCR sharing between clusters in the combined 6

170 and 41 wpi dataset (Fig.2B). There was significant clonotype sharing between $T_{EFF}/0$ and T_{SL}-

171 M/2 or TPOLY/6, and little or no sharing with TEXH/1. The relation between the clusters was

172 independently assessed by pseudotime analysis using Monocle3 (*59, 60*) with TN/3 as the root

173 cells. Path 1 led to functional branch, including TEFF/0, TSL-M/2, TRM/4, TPOLY/6 (hereafter,

174 referred to as 'TEFF/TRM branch') while Path 2 led to TEXH/1 (hereafter, referred to as 'TEXH

175 branch') (Fig.2C). Interestingly, TIFN/8 cells are derived from the TEFF/TRM branch at 6 wpi, but

176 they are derived from the TEXH branch at 41 wpi (Fig.2C). TEFF/0, TRM/4, and TPOLY/6, cluster

177 separately and distantly from TEXH/1, and have little TCR overlap. This is consistent with previous

178 observations that T cell exhaustion represents a distinct T cell differentiation program from the

179 effector differentiation program (*61, 62*). In contrast, CD8$^+$ T cells in TSL-M/2 could give rise to

180 TEFF/0 and TPOLY/6 based on TCR sharing and pseudotime analysis. Thus, CD8$^+$ T cells follow

181 at least two divergent differentiation trajectories with different functional fates.

182 We next sought to identify the most differentially expressed genes (DEGs) between the

183 TEFF/TRM and the TEXH branch. We identified 267 DEGs (Fig.2D, Table S3). Cells on the TEXH

184 branch are enriched for *Tox, Gzmk, Tigit, Pdcd1, Eomes, Il10ra, Ccl5,* and *Cd27.* Cells on the

185 TEFF/TRM branch are enriched for *Cd226, Ifng, Tnf, Jaml, Klrg1,* and *Il18r1*. Remarkably, *Cd226*

186 is the top DEG enriched in TEFF/TRM branch. Together with *Ifng*, *Cd226* distinguishes CD8$^+$ T

187 cells in TEFF/TRM branch from those expressing high levels of *Gzmk* and exhaustion-related

188 genes, including *Tigit, Pdcd1, Tox*, and *Eomes* (Fig.2D, E).

189

Cd226 expression is associated with CD8$^+$ T cell effector responses

191 To substantiate our finding that *Cd226* distinguishes between two distinct CD8$^+$ T cell

192 lineages (i.e., TEFF/TRM vs. TEXH), lung parenchymal CD226$^+$ or CD226$^-$ CD44$^+$CD8$^+$ T cells were

193 purified from infected mice and analyzed by bulk RNAseq (Fig.S2A; Table S4). We observed 202

194 DEGs between CD226$^+$ and CD226$^-$ CD8$^+$ T cells (Fig.3A). The CD226$^+$CD8$^+$ T cells expressed

195 higher levels of genes associated with effector function (*Ifng*), terminal differentiation (*Klrg1*,

196 *Havcr2*), and proliferation (*Mki67, Top2a*). Gene set enrichment analysis (GSEA) confirmed that

197   CD226$^+$CD8$^+$ T cells were enriched in signatures related to effector CD8$^+$ T cells (Fig.3B). In

198   contrast, the CD226$^-$ CD8$^+$ T cells expressed genes associated with T cell exhaustion (*Pdcd1,*

199   *Tox*). To further corroborate the correlation of *Cd226* expression with features of effector cells,

200   we reanalyzed scRNA-Seq data using Monocle3 and identified 49 modules of coregulated DEGs

201   (Table S5). Module 22 is enriched in the T$_{EFF}$/T$_{RM}$ lineage (Fig.S2B), includes the GO terms

202   "regulation of immune effector process," "leukocyte migration," "interferon−gamma production,"

203   and "regulation of cytokine production involved in immune response" (Fig.S2C), and includes

204   *Cd226*. Thus, *Cd226* expression identifies CD8$^+$ T cells with effector program that undergo

205   terminal differentiation, express high *Ifng*, and resist the expression of exhaustion-associated

206   genes including *Tox* and *Pdcd1*.

207   We next asked whether *Cd226* expression by CD8$^+$ T cells is altered during other chronic

208   diseases. CD8$^+$ T cells in LCMV Clone 13 infection and tumor models exhibit distinct functional

209   phenotypes defined by two co-inhibitory receptors: PD-1 and TIM-3. After LCMV Clone 13

210   infection, *Cd226* expression by CD8$^+$ T cells is associated with a terminally exhausted PD-1$^+$TIM-

211   3$^+$ phenotype (*63*)(Fig.3C). The results in the CT26 colon carcinoma model are not as clear, but

212   *Cd226* expression is biased towards terminally exhausted PD-1$^+$TIM-3$^+$ CD8$^+$ T cells (Fig.3C)(*64*).

213   In contrast, reanalysis of our previous data finds that during TB, *Cd226* is mostly expressed by

214   PD1$^-$TIM3$^+$ CD8$^+$ T cells and not terminally exhausted PD-1$^+$TIM-3$^+$ T cells (*29*) (Fig.3C). Thus,

215   the pattern of *Cd226* expression by CD8$^+$ T cells with effector features but not exhausted CD8$^+$ T

216   cells during Mtb infection differs from its expression during chronic LCMV infection or cancer.

217   Furthermore, PD1$^-$TIM3$^+$ CD8$^+$ T cells, which are abundant during Mtb infection, are poorly

218   described in chronic LCMV or tumor models (*64, 65*). In summary, *Cd226* expression identifies

219   CD8$^+$ T cells with an effector program during Mtb infection.

220

221   **CD226$^+$CD8$^+$ T cells express more IFNγ in vivo.**

222   As *Cd226* is highly expressed by CD8$^+$ T cells with effector program at the RNA level, we

223 next measured its cell surface expression by naïve splenic CD8$^+$ T cells and lung CD8$^+$ T cells

224 isolated at 4, 11, 21, 30, and 43 wpi (Fig.4A, B, C). As previously reported, nearly all CD8$^+$ and

225 20-40% of CD4$^+$ splenic T cells from uninfected mice express CD226 by flow cytometry (Fig.4A,

226 B). In the lungs of infected mice, 90-100% of parenchymal (CD45-IV$^-$) antigen-experienced CD44$^+$

227 CD62L$^-$ CD8$^+$ T cells initially express CD226; however, CD226 expression steadily declines

228 during chronic infection (Fig.4A, B). After 40 wpi, ~40% of parenchymal CD8$^+$ T cells lack CD226

229 expression. In contrast, 50~85% of CD4$^+$ T cells express CD226, which fluctuates over the course

230 of infection, but does not change significantly. Compared to naïve CD44$^-$CD62L$^+$ CD8$^+$ T cells,

231 antigen-experienced CD44$^+$CD62L$^-$ CD8$^+$ T cells increase CD226 expression levels after infection

232 (Fig.4C). CD226 is highly expressed by CD4$^+$ and CD8$^+$ T cells, but also γδ T and NK cells

233 (Fig.S3A, B). Like in the lung, CD8$^+$ T cells in the mediastinal lymph nodes (LN) and spleens of

234 Mtb-infected mice gradually lose CD226 expression over time (Fig.S3C). Thus, CD226 is highly

235 expressed by lung parenchymal CD8$^+$ T cells, consistent with our scRNAseq data, and its

236 expression decreases over time during Mtb infection.

237   As CD226 marks CD8$^+$ T cells with effector programs both early and late during TB (Fig.2,

238 3), we wished to further characterize how the activation state of CD226$^+$ and CD226$^-$ CD8$^+$ T cells

239 differ. To assess IFNγ production by T cells "in vivo" without the need for ex vivo restimulation,

240 we infected IFNγ-IRES-eYFP (GREAT) reporter mice (66) with Mtb. We validated comparable

241 expression levels of IFNγ–eYFP and IFNγ protein in response to anti-CD3 and anti-CD28 mAb

242 stimulation in both CD4$^+$ and CD8$^+$ T cells, in line with published data (67) (Fig.S4). Although an

243 IFNγ-reporter will miss CD8$^+$ T cells expressing non-cytokine functions, we previously found that

244 nearly all cytokine-producing CD8$^+$ T cells in the lungs of Mtb-infected mice produce IFNγ (68).

245 Between 10-75% of lung parenchymal CD4$^+$ and CD8$^+$ T cells in the lung produce IFNγ-eYFP

246 and their frequency peaks at 23-36 wpi (Fig.4D). While both intravascular (IV$^+$) and parenchymal

247 (IV$^-$) CD4$^+$ T cells are IFNγ-eYFP$^+$, only IV$^-$ CD8$^+$ T cells are IFNγ-eYFP$^+$ (Fig.4D). Based on

248 eYFP MFI, more IFNγ is made by CD226$^+$ than CD226$^-$ CD8$^+$ T cells (Fig.4E), and when IFNγ-

249 eYFP levels peak around 20-36 wpi (Fig.4D), higher percentages of CD226$^+$CD8$^+$ T cells express

250 IFNγ-eYFP than CD226$^-$CD8$^+$ T cells (Fig.4E, F). Thus, using IFNγ-reporter mice, we established

251 that CD226 identifies IFNγ-producing CD8$^+$ T cells in the lungs of Mtb-infected mice in vivo.

252

253 **CD226 distinguishes phenotypically and functionally distinct CD8$^+$ T cell populations**

254 To confirm our transcriptional analysis and understand how CD226$^+$ and CD226$^-$ lung

255 parenchymal CD8$^+$ T cells differ functionally, we used flow cytometry to measure the expression

256 of well-defined phenotypic markers. Compared to CD226$^-$CD8$^+$ T cells, CD226$^+$CD8$^+$ T cells

257 express more KLRG1, TIM-3, IL-18Rα, CD103, and produce more IFNγ (Fig.5A, B, Fig.S5A).

258 KLRG1 and CD103 expression by CD226$^+$CD8$^+$ T cells are mutually exclusive and, as suggested

259 by our scRNAseq data, divides CD226$^+$CD8 T cells into two differentiated subsets: KLRG1$^+$

260 (TEFF/0) and CD103$^+$ (TRM/4) (Fig.5A, B; Fig.S5B). While T-bet levels were greater in

261 CD226$^+$CD8$^+$ T cells, Eomes levels were higher in CD226$^-$CD8$^+$ T cells, consistent with a previous

262 finding of Eomes-dependent CD226 loss in tumors (Fig.5C, S5C) (*37*).

263 Over time, more CD226$^-$CD8$^+$ T cells express PD-1, and those that do, express higher

264 PD-1 levels than CD226$^+$ CD8$^+$ T cells (Fig.5D; Fig.S5D). PD-1 expression by CD226$^+$CD8$^+$ T

265 cells is limited but preferentially expressed on CD103$^+$ cells (Fig.5A), consistent with enrichment

266 of an exhaustion gene signature in TRM/4 (Fig.1F, G). When we divide CD8$^+$ T cells based on PD-

267 1 and TIM-3 expression, PD-1$^-$TIM-3$^+$ cells are evident after 9 wpi, and these cells have the

268 highest CD226 levels, especially late during infection (Fig.S5E), consistent with our transcriptomic

269 data (Fig.3C) (*29*). TIGIT expression was constantly higher in CD226$^-$CD8$^+$ T cells than in

270 CD226$^+$CD8$^+$ T cells throughout the infection (Fig.5D, Fig.S5D).

271 We next compared the potential of lung parenchymal CD226$^+$ and CD226$^-$ CD44$^+$CD8$^+$ T

272 cells to produce cytokines after ex vivo restimulation with anti-CD3 and anti-CD28 antibodies.

273 Sorted CD226$^+$CD8$^+$ T cells from the lungs of Mtb-infected mice were more polyfunctional

274 (IFNγ$^+$TNF$^+$IL-2$^+$ or IFNγ$^+$TNF$^+$IL-2$^-$) than CD226$^-$CD8$^+$ T cells, independent of the duration of

275   infection (Fig.5E). Conversely, a higher percentage of CD226$^-$CD8$^+$ T cells produced only IFNγ

276   or were IFNγ$^-$TNF$^-$IL-2$^-$, compared to CD226$^+$CD8$^+$ T cells.

277   We next asked whether CD226 expression identifies Mtb-specific effector CD8$^+$ T cells.

278   TB10.4$_{4-11}$ and 32A$_{309-318}$ are immunodominant epitopes recognized by CD8$^+$ T cells from

279   C57BL/6J mice. TB10.4-specific CD8$^+$ T cells maintain CD226 expression in the lung and other

280   tissues even very late during chronic infection (Fig.5F; Fig.S5F). Similarly, nearly all 32A-specific

281   CD8$^+$ T cells express CD226 throughout the infection (Fig.5G).

282   Thus, cell surface CD226 expression distinguishes two major CD8$^+$ T cell populations in

283   the lung during Mtb infection. CD226$^+$CD8$^+$ T cells are the dominant population, which include

284   terminally differentiated CD8$^+$ T cells that express KLRG1 (T$_{EFF}$/0) or CD103 (T$_{RM}$/4) and are

285   capable of polyfunctional cytokine production. In contrast, CD226$^-$CD8$^+$ T cells emerge as early

286   as 4 wpi, are primarily in the T$_{EXH}$/1 cluster, express PD-1, TIGIT, and Eomes, and have a

287   reduced potential for polyfunctional cytokine production. Thus, the absence of CD226 expression

288   by CD8$^+$ T cell is an indication of CD8$^+$ T cell exhaustion during TB.

289

290   CD226 costimulates CD8$^+$ T cell recognition of Mtb-infected macrophages

291   As CD226 identifies Mtb-specific polyfunctional CD8$^+$ T cells, we sought to determine if

292   CD226 functions in recognizing Mtb-infected macrophages. The binding of CD226 to its ligands

293   CD155 (Poliovirus receptor, PVR) or CD112 (Nectin-2) costimulates both T cells and NK cells

294   (*33, 69-71*). We assessed the expression of CD226 ligands by antigen-presenting cells. CD155

295   is expressed by nearly all alveolar macrophages (AM) and non-AM macrophages and 60% of

296   monocytes and dendritic cells in the lungs of infected mice (Fig.6A, Fig.S6A). CD112 is expressed

297   by 60% of alveolar and non-alveolar macrophages and 20-50% of monocytes and dendritic cells.

298   Like lung macrophages, uninfected and infected thioglycolate-elicited peritoneal macrophages

299   (TG-PMs), which are inflammatory recruited macrophages, expressed uniformly high levels of

300   CD155 and lower levels of CD112 (Fig.6B).

301   To compare the capacity of CD226$^+$ and CD226$^-$ CD8$^+$T cells to recognize Mtb-infected

302   macrophages, CD45-IV$^-$CD44$^+$CD8$^+$ T cells from the lungs of infected mice were sorted into

303   CD226$^+$ or CD226$^-$ populations and cultured with infected TG-PMs (Fig.S6B). More CD226$^+$ CD8$^+$

304   T cells recognized Mtb-infected macrophages than CD226$^-$ CD8$^+$T cells, based on IFNγ and TNF

305   production measured by ICS, at all multiplicities of infection (MOI) tested (Fig.6C, D, Fig.S6C).

306   Importantly, the recognition of Mtb-infected macrophages was specific, as there was little cytokine

307   production when CD226$^+$ CD8$^+$ T cells were cocultured with MHC-mismatched Mtb-infected TG-

308   PMs from BALB/cJ mice.

309   We next investigated whether CD226 is involved in the interaction between T cells and

310   infected macrophages. Sorted lung parenchymal CD226$^+$ or CD226$^-$ CD44$^+$CD8$^+$ T cells from

311   infected mice (12, 20, and 28 wpi) were cultured with Mtb-infected macrophages in the presence

312   or absence of a blocking anti-CD226 mAb. Anti-CD226 mAb inhibited IFNγ production by CD226$^+$

313   CD8$^+$ T cells (Fig.6E, Fig.S6C). Additionally, CD226 blocking reduced soluble Gzmb levels

314   detected after CD8$^+$ T cell culture with infected macrophages, suggesting reduced cytotoxicity

315   (Fig.6F). We conclude that CD226 is a marker for CD8$^+$ T cells that recognize Mtb infected

316   macrophages and functions as a costimulatory molecule in activating CD8$^+$ T cells following MHC-

317   restricted recognition of infected macrophages.

318

_CD226_ and _GZMK_ identify distinct CD8$^+$ T cell subsets from macaques and humans

320   We next determined if _CD226_ expression is associated with effector CD8$^+$ T cells in other

321   species using published scRNA-Seq datasets of CD8$^+$ T cells obtained from the lungs of Mtb-

322   infected cynomolgus macaques and people. Previously, CD8$^+$ T cells from TB granulomas in the

323   lungs of macaques after primary infection were categorized into four subsets (72): 1) TEMRA-

324   like; 2) Eff-like; 3) GZMK^{hi} TEM/PEX-like (GZMK^{hi}); and 4) Tc17-like. These CD8$^+$ T cells

325   (n=3,974) were reanalyzed for _CD226_ expression. _CD226_ is high in TEMRA-like and Eff-like cells

326   and lowest in GZMK^{hi} CD8$^+$ T cells (Fig.7A). Reanalyzing DEGs between _CD226_^{hi} (TEMRA-like,

327   Eff-like, and Tc17-like) and $CD226^{lo}$ ($GZMK^{hi}$) CD8$^+$ T cells highlighted the mutually exclusive

328   expression of *CD226* and *GZMK* by CD8$^+$ T cells (Fig.7B, Table S6). *CD226* was associated with

329   the expression of *CX3CR1*, which is associated with tissue residency, and the cytotoxic effector

330   molecules *GZMA, GZMB, PRF1*, and *GNLY*; in contrast, *GZMK* was associated with *CD28,*

331   *EOMES,* and *TOX* expression. Reanalysis of granuloma CD8$^+$ T cells at a later time point, from

332   another Mtb-infected cynomolgus macaque dataset found *CD226* expression to be exclusively

333   high in cytotoxic cluster 4, which was previously identified as being associated with low-bacterial-

334   burden granulomas (Fig.7C)(*5*). We observed the same dichotomy of *CD226* and *GZMK*

335   expression on cytotoxic cells in reanalyzing DEGs between cytotoxic cluster 4, which has the

336   highest *CD226* expression, and other cytotoxic clusters, which had little *CD226* expression

337   (Fig.7D, Table S6). *CD226* was associated with the expression of *CX3CR1*, and *GZMK* was

338   associated with the expression of *CD28*, *EOMES*, *TIGIT, GZMA,* and *GNLY* (Fig.7D). We further

339   confirmed this dichotomic expression of *CD226* and *GZMK* on lung granuloma CD8$^+$ T cells

340   (n=1,510) from another cynomolgus dataset (*11*). We used 0.5 as a log normalized expression

341   threshold to divide cells into CD226^{hi} (n=609) and CD226^{lo} (n=901) CD8$^+$ T cells. *CD226* was

342   associated with the expression of *IFNG* and *TNF* and the cytotoxic molecules *PRF1* and *GZMB*

343   on CD8$^+$ T cells (Fig.7E, Table S6). *GZMK* was associated with the expression of *EOMES*, *TOX*,

344   and *TIGIT* (Fig.7E). Thus, lung granuloma *CD226*-expressing CD8$^+$ T cells from infected

345   macaques have effector features marked by the expression of *CX3CR1* and cytotoxic effector

346   molecules and cytokines. In contrast, *GZMK* was associated with the expression of exhaustion-

347   associated genes, including *EOMES* and *TOX*. Finally, we reanalyzed 7,241 CD8$^+$ T cells from

348   the resected lungs of patients with active TB (*73*). DEGs between CD226^{hi} (n=661) and CD226^{lo}

349   (n=6,580) CD8$^+$ T cells using 0.5 as a log normalized expression threshold to divide cells, the

350   same dichotomy was observed between *CD226* and *GZMK* expression (Fig.7F, Table S6).

351   *CD226*-expressing cells have enriched expression of *ZNF683*, which is related to tissue

352   residency, and *GZMB* and *GNLY,* which encode cytotoxic effector molecules. Taken together,

353   *CD226* and *GZMK* expression identify distinct CD8$^+$ T cell subsets in the Mtb infected lung. Thus,

354   CD226 expression identifies CD8$^+$ T cells with effector features, in mice, macaques, and humans.

355 **Discussion.**

356 Recognition of Mtb-infected macrophages is crucial during CD8$^+$ T cell mediated immunity

357 during TB (*17, 23*). We previously found that some CD8$^+$ T cells inefficiently recognize Mtb-

358 infected cells by their IFNγ secretion, but the mechanisms are poorly understood (*21, 22, 24*). To

359 determine whether heterogeneity among CD8$^+$ T cells could explain the variation in recognition

360 of Mtb-infected macrophages and inhibition of Mtb growth that is observed experimentally, we

361 analyzed lung parenchymal (i.e., extravascular) CD8$^+$ T cells by scRNA-seq, paired TCR-seq,

362 and high dimensional flow cytometry with IFNγ-eYFP reporter mice. We identified distinct CD8$^+$ T

363 cell clusters containing clonally expanded T cells and defined functional (T$_{EFF}$/0, T$_{RM}$/4, and

364 T$_{POLY}$/6) and dysfunctional (T$_{EXH}$/1 and T$_{IFN}$/8) states, at 6- and 41-weeks after infection. An

365 important discovery is that CD226 expression distinguishes effector CD8$^+$ T cells with retained

366 polyfunctionality from dysfunctional CD8$^+$ T cells throughout Mtb infection. Importantly, CD8$^+$ T

367 cell with dysfunctional states, characterized by the lack of CD226 expression, did not recognize

368 infected macrophages. On the other hand, CD8$^+$ T cells with functional states characterized by

369 CD226 expression, recognized infected macrophages in an MHC-restricted manner, and blocking

370 CD226 diminished recognition. CD226 is a T cell activation marker, functions as an adhesion

371 molecule, and costimulates T cells (*33, 69, 70, 74*). Costimulation occurs when CD226 binds to

372 CD155 or CD112 (*71*). Our work highlights a novel role of the CD226 costimulatory signal in

373 enhancing CD8$^+$ T cell recognition of Mtb-infected macrophages.

374 CD226 signaling by tumor-infiltrating CD8$^+$ T cells is negatively regulated by PD-1 and

375 TIGIT(*75*). PD-1 inhibits the phosphorylation of CD226 via its ITIM-containing intracellular domain

376 (*75*). TIGIT competes with CD226 for binding to CD155, and ligation to CD155 induces

377 internalization and degradation of CD226 as a possible negative feedback mechanism (*35*). The

378 loss of the expression or signaling of CD226 restrains CD8$^+$ T cell functions, leads to the

379 accumulation of dysfunctional CD8$^+$ T cells in the tumor microenvironment, and is associated with

380 impaired tumor control (*35*). In the setting of cancer, PD-1 and TIGIT are often co-expressed with

381   CD226 on CD8$^+$ T cells, and CD226 expression is required for response to anti-PD-(L)1 or anti-

382   TIGIT antibody treatment (*36, 37, 75*). However, during chronic TB, PD-1 and TIGIT are

383   expressed at low levels on CD226$^+$ CD8$^+$ T cells. Dysfunctional CD8$^+$ T cells that have entirely

384   lost CD226 expression now express high levels of PD-1 and TIGIT. This distinct expression

385   pattern of PD-1, TIGIT, and CD226 might explain distinct outcome induced by PD-1 blockade in

386   TB (*76*). In a murine cancer model, additional mechanisms occur at the transcriptional level to

387   restrict CD226 expression, where Eomes promote CD226 loss by tumor-infiltrating CD8$^+$ T cells

388   (*37*). In our study, like in cancer, CD226$^+$CD8$^+$ T cells have high T-bet and low Eomes expression,

389   while CD226$^-$CD8$^+$ T cells have low T-bet and high Eomes levels, suggesting that balance of T-

390   bet and Eomes affects CD226 expression during TB (*37*).

391   Surprisingly, we found a distinct TIM-3 expression pattern on CD8$^+$ T cells during Mtb

392   infection. While TIM-3$^+$PD-1$^-$ CD8$^+$ T cells are not detected in cancer or chronic LCMV infection,

393   in chronic Mtb infection, nearly 25% of the CD8$^+$ T cells are TIM-3$^+$PD-1$^-$, and this subset has

394   high CD226 levels and an effector state. This is consistent with TIM-3 signaling driving stronger

395   effector functions in CD4$^+$ and CD8$^+$ T cells in Mtb infected mice(*29*) and active TB patients (*77*).

396   TIM-3 is recruited to the immune synapse and enhances phosphorylation of ribosomal S6 protein

397   and Akt/mTOR signaling under acute stimulation such as during *Listeria monocytogenes* infection

398   (*78-81*). Sustained expression of TIM-3 with PD-1 is associated with terminally exhausted CD8$^+$

399   T cells during cancer and chronic LCMV infection (*65, 82*). While robust TIM-3 upregulation in the

400   absence of PD-1 on CD8$^+$ T cells is also observed during *Mycobacterium avium* infection (*83*),

401   and TIM-3$^+$PD-1$^-$ CD8$^+$ T cells are also found in HIV-1 and HCV infection (*84, 85*), the functionality

402   of TIM-3$^+$PD-1$^-$ CD8$^+$ T cells are poorly described. Our data support the costimulatory role of TIM-

403   3 to help effector function in the absence of PD-1 during Mtb infection.

404   There are parallels between how CD226 and CD28 costimulate T cells and are regulated.

405   Both are immunoglobulin superfamily members that bind ligands on APCs (CD155 or CD112, and

406   CD80 and CD86, respectively). Coinhibitory receptors compete for ligand binding as a mechanism

407   to down-regulate or terminate T cell responses. TIGIT competes for CD155 binding, while CTLA4

408   competes for CD28 binding. Both CD226 and CD28 are regulated by PD-1 signaling (*75*). These

409   mechanistic insights led to the discovery that successful checkpoint blockade targeting PD-1 and

410   TIGIT during cancer depends on the presence of CD226$^+$CD8$^+$ T cells (*36, 37, 75*). CD226 and

411   CD28 have opposite expression patterns in two cynomolgus macaque datasets. Thus, CD226

412   could also be an important costimulatory molecule for macaque CD8$^+$ T cells during Mtb infection.

413   Finally, we find an interesting dichotomy between CD226 and GZMK expression among CD8$^+$ T

414   cells. Although GZMK, in combination with perforin, has cytolytic and anti-mycobacterial activity

415   in vitro (*86*), in our dataset, it is associated with the two dysfunctional clusters, T$_{EXH}$/1 and T$_{IFN}$/8.

416   In scRNA-Seq data from all species (mouse, cynomolgus macaque and human), *GZMK* is

417   expressed by CD226^{lo}CD8$^+$ T cells. In Mtb-infected cynomolgus macaques, a population of

418   CD226^{lo}CD8$^+$ T cells express high *GZMK* levels together with *TIGIT, EOMES, TOX,* and *CD28*

419   (*72*). Interestingly, a higher proportion of lung granuloma cytotoxic 4 cells from Gideon *et al.* (*5*),

420   which have exclusive expression of *CD226*, were associated with Low-bacterial-burden

421   granulomas, but cytotoxic 5 cells, which are distinguished by elevated expression of *GZMK*, did

422   not associate with bacterial control (*5*). The functional role of GZMK-expressing CD8$^+$ T cells

423   during TB requires further investigation.

424   We do not yet know whether CD226 expression on CD8$^+$ T cells promotes protection

425   against TB. CD226 blockade in vitro diminishes IFNγ and granzyme B production by CD8$^+$ T cells.

426   If CD226 costimulates cytokine production and cytotoxic functions of CD8$^+$ T cells in vivo, we

427   predict that CD226 signaling would reduce the survival of intracellular Mtb in macrophages. As

428   CD226 is involved in priming (*70*), it might have a role in the robust expansion and maintenance

429   of CD226$^+$CD8$^+$ T cells during infection. Further study using CD226 knockout mice to investigate

430   its role in priming, expansion, and control against infected cells can elucidate its contribution to

431   protective CD8$^+$ T cell immunity in TB. In conclusion, we identified CD226 as a functional marker

432   that identifies effector CD8$^+$ T cells with the capacity to recognize infected macrophages. We

433   predict that CD226 will identify effector CD8$^+$ T cells in cynomolgus macaques and humans based

434   on analysis of transcriptional data. As CD226 is lost by dysfunctional CD8$^+$ T cells, changes in its

435   expression might be useful in evaluating impaired CD8$^+$ T cell responses and disease progression

436   in clinical settings. Finally, the CD226-CD155/CD112 axis should be considered as a strategy to

437   enhance immune responses induced by vaccination (*87*).

438

Methods.

Ethics statement

Studies were conducted using the relevant guidelines and regulations and approved by the Institutional Animal Care and Use Committee at the University of Massachusetts Medical School (UMMS) (Animal Welfare A3306-01), using the recommendations from the Guide for the Care and Use of Laboratory Animals of the National Institutes of Health and the Office of Laboratory Animal Welfare.

Mice

C57BL/6J, BALB/cJ and IFNγ-IRES-eYFP reporter (GREAT) mice (*66*) (Strain #017580) were purchased from The Jackson Laboratory. The mice used in this study were 6–8-week-old in the animal facility at the UMass Chan Medical School. Mice of both sexes were used and the experiments reported herein did not test sex as a variable.

Mtb strain

The Erdman strain was used for aerosol infection (*88*). H37Rv-pLux or Rv.YFP strain (H37Rv expressing yellow fluorescent protein (YFP)(*89*) were used to infect macrophages *in vitro*.

Aerosolized Mtb infection of mice

Mice were infected by the aerosol route as previously described(*89*). Briefly, frozen bacterial stocks were thawed and added to 3 ml of 0.01% Tween-80 in PBS. The bacteria were sonicated for 1 minute, and 2 ml of 0.01% Tween-80 in PBS were added. To infect mice, the bacterial suspension was aerosolized using a Glas-Col chamber (Terre Haute). The average number of bacteria delivered into the lung was determined for each experiment by plating lung homogenate on 7H11 plates (Hardy Diagnostics) from 5 mice within 24 hours after infection and ranged between 50-200 CFU/mouse.

465

Cell isolation

Mtb-infected C57BL/6J mice were injected intravenously with 2.5 µg of fluorochrome-labeled anti-CD45.2 3 minutes before euthanasia and lung removal. Single cell suspensions were prepared by homogenizing lungs using a GentleMACS tissue dissociator (Miltenyi), digesting with 300 U/ml Type IV Collagenase (Sigma-Aldrich, C5138-5G) in complete RPMI (RPMI-1640 medium supplemented with 10% FBS, 1× Non-Essential Amino Acids (Gibco, 11140050) and 10 mM HEPES (Gibco, 15630080), 2 mM L-Glutamine (Gibco, 25030081), 100 units/ml Penicillin–Streptomycin (Gibco, 15140122), 0.5X MEM Amino Acids (Gibco, 11130051), and 55µM 2-Mercaptoethanol (Gibco, 21985023)) at 37°C for 30 minutes, and followed by a second run of dissociation using the GentleMACS. Suspensions were filtered through 70-µm strainers, and red blood cells were lysed in ACK Lysis Buffer (Gibco; Thermo Fisher Scientific). Suspensions were then filtered through 40-µm strainers. Mediastinal LN or spleen were harvested, mashed with a 3-ml syringe on a 24-well plate with RPMI 1640, filtered with 70-µm strainers, washed with RPMI-1640, and resuspended with autoMACS running buffer (Miltenyi).

480

Flow cytometry

Single-cell suspensions, prepared as described earlier in Cell isolation section, were stained with Zombie Fixable Viability dye (Biolegend) in PBS for 10 minutes at room temperature (RT). After washing cells with autoMACS running buffer, cells were incubated with anti-mouse CD16/32 (BioXcell) for 5 minutes, followed by surface staining performed for 20 min at 4°C in autoMACS running buffer. TB10.4$_{4\text{-}11}$ and/or 32A$_{309\text{-}318}$ tetramers were stained together with antibodies for surface staining. The following antibodies were used: Anti-mouse CD90.2 (53-2.1), CD8b (YTS156.7.7), CD8a (53-6.7), CD4 (RM4-5 or GK1.5), CD45R/B220 (RA3-6B2), CD3 (17A2), CD44 (IM7), TIGIT/Vstm3 (1G9), CD279/PD-1 (29F.1A12), CD366/Tim-3 (RMT3-23), NK-1.1 (PK136), CD155/PVR (TX56), CD226 (10E5), CD218a/IL-18Rα (A17071D), TCRβ chain (H57-

491 597), KLRG1/MAFA (2F1/KLRG1), CD103 (2E7), CD11c (N418), CD11b (M1/70), MERTK/Mer

492 (2B10C42), Ly-6G (1A8), CD64 (X54-5/7.1), CD19 (1D3/CD19), IFN-γ (XMG1.2), TNF-α (MP6-

493 XT22), IL-2 (JES6-5H4), T-bet (4B10) (all from BioLegend). Anti-mouse Siglec-F (E50–2440),

494 CD45.2 (104), CD112/Nectin-2 (829038), CD62L (MEL-14), γδ T-Cell Receptor (GL3) were

495 obtained from BD Biosciences, and Eomes (Dan11mag) was obtained from Invitrogen. After

496 washing with autoMACS running buffer, stained cells were fixed in 1% paraformaldehyde.

497 Samples were assessed on a Cytek Aurora (Cytek). Flow cytometry data were processed and

498 analyzed using FlowJo software (BD bioscience) and FlowJo plugins UMAP v4.1.1. Lung

499 parenchymal $CD8^+$ T cells were defined as intravascular (IV) $CD45^-$, $CD90.2^+CD4^-CD8\alpha^+CD8\beta^+$.

500 2,294 lung parenchymal antigen-experienced ($CD44^+CD62L^-$) $CD8^+$ T cells from each mouse

501 (n=3/time point) were used for concatenation to one FCS file before creating UMAP projections.

502

503 **Cell Sorting**

504 Cells were prepared as described earlier in Cell isolation section. Dead cells were removed using

505 EasySep™ Dead Cell Removal (Annexin V) Kit (Stemcell) before staining. Cell staining was

506 performed as described earlier in the Flow cytometry section. Stained cells were sorted by MA900

507 Multi-Application Cell Sorter (Sony).

508

509 **scRNA-seq library preparation**

510 Lung single cell suspensions were prepared as above in Cell isolation section, and T cells from

511 individual C57BL/6J mice were sorted based on $CD45-IV^-CD3^+TCR\beta^+$ (n=2 at 6 wpi; n=2 at 41

512 wpi). Antibodies for NK1.1, CD19 and TCRγδ were used for the "dump" channel. 10,000 flow-

513 sorted T cells from mouse were loaded into a single Chip channel (10× Chromium). Gel beads-

514 in-emulsion (GEM) generation, cDNA amplification, and library construction were performed using

515 Chromium Single Cell 5' Library Construction Kit (v2 Chemistry Dual Index). Chromium Single

516 Cell V(D)J Enrichment Kit, Mouse T Cell were used to generate TCR Libraries. The final libraries

517   were sequenced on the Illumina NextSeq 500 platform.

518

519   **scRNA-seq data processing and analysis**

520   Sequencing reads were mapped to mouse reference genome GRCm38 (mm10) and processed

521   through CellRanger (v6, 10× Genomics). All downstream analyses were performed through

522   Seurat (v.4.1.1) for R (v4.2.0). Low-quality cells where >10% of transcripts derived from the

523   mitochondria were excluded. The data was filtered to retain cells with 300-5,000 genes detected

524   and UMI counts of 500-25,000. The TCR genes (Tra[vjc], Trb[vdjc], Trg[vj], Trd[vdjc]) were

525   removed for from the gene expression dataset to avoid any TCR gene-driven bias during

526   clustering. CD8$^+$ T cells were selected based on Cd4 < 1e-10 AND Cd8a > 0.5 AND Cd8b1 > 0.5

527   AND Cd3e > 1. SCTransform normalization was performed. Linear dimensional reduction was

528   performed using *RunPCA* with argument npcs = 30, *RunUMAP*, *FindNeighbors,* and *FindClusters*

529   with argument resolution = 0.9. DoubletFinder (v2.0.3), assuming a theoretical doublet rate of 0.8-

530   4.6% depend on the samples, was additionally used to remove doublets. Resulting doublets were

531   0.3-4.1%. To combine data across all samples, highly variable 3000 genes were selected for

532   anchoring using the *SelectIntegrationFeatures* function, and integration was performed using

533   *PrepSCTIntegration*, *FindIntegrationAnchors,* and *IntegrateData* functions. *RunUMAP* was

534   performed on the integrated dataset, followed by *FindNeighbors* (reduction = "pca") using the first

535   10 principal components. *FindClusters* (resolution = 0.3) was performed, and 9 clusters were

536   identified. The cluster markers were found using the *FindAllMarkers* function (min.pct = 0.25,

537   assay = "RNA"), and avg_log2 fold change (FC) and adjusted P value are shown in Table S1.

538   Barplot was visualized by dittoseq (v1.10.0). Volcanoplots were created with the R package

539   EnhancedVolcano (v1.16.0).

540

541   **Gene signature scoring**

542   We computed average gene expression scores for published gene sets with *AddModuleScore*

543   function in Seurat (v.4.1.1).

544

Projection of published scRNA-seq data to our scRNA-seq data

546   Published processed Seurat object (*58*) was used as a reference to apply label transfer to our

547   dataset using *ProjecTILs.classifier* function in ProjecTILs (v3.3.0).

548

Pseudotime trajectory analysis

550   To determine the potential development lineages of CD8$^+$ T cell clusters, we used Monocle3

551   (v.1.3.1) on the integrated Seurat object. Using the SeuratWrappers package, we converted the

552   integrated Seurat object to a cell dataset object. We selected the naive T cell cluster (T$_N$/3) as the

553   root for the trajectory. Cells were clustered with *cluster_cells* using "Louvain" as a cluster_method.

554   Two separate partitions for the clusters were detected, and the partition with the proliferating CD8$^+$

555   T cells (T$_{PROLIF}$/7) was excluded from the pseudotime trajectory analysis. Trajectory graph learning

556   and pseudotime measurement were performed using *learn_graph* and *order_cells* function. Next,

557   we used the *graph_test* function to identify genes that are differentially expressed on different

558   paths through the trajectory. The genes that had a significant q-value (<0.05) from the

559   autocorrelation analysis were grouped into 49 distinct co-regulated modules using

560   *find_gene_modules* function (resolution=1e-2) (Table S5). The *aggregate_gene_expression*

561   function was used to calculate aggregate expression of genes in each module for all the clusters.

562   We used the *enrichGO* function in the clusterProfiler package (v 4.6.2) to measure the enrichment

563   of the modules in GO terms across all three ontologies ("BP," "MF," and "CC").

564

Cytokine signaling activity score

566   The cytokine signaling activity of each Seurat cluster on the integrated scRNA-Seq data was

567   predicted using CytoSig(*53*). Averaged gene expression on 2000 variable genes of all cells in

568   each Seurat cluster was calculated using *AverageExpression* function (assays = "RNA").

569 Predicted cytokine signaling activity scores were calculated in CytoSig

570 (https://cytosig.ccr.cancer.gov/) and plotted in a heatmap using the R package ComplexHeatmap

571 (v2.14.0)

572

573 **SCENIC regulons**

574 R package SCENIC (v1.3.1) was used for GRN inference. For efficient analysis, the integrated

575 scRNA-Seq dataset was down-sampled to 3000 cells. We created the initialize settings

576 configuration object with *initializeScenic* function with default settings. To remove genes that are

577 expressed either at very low levels or in too few cells, we only kept the genes with at least 6 UMI

578 counts, detected in at least 1% of the cells, and are available in RcisTarget databases. After

579 calculating the spearman correlation with *runCorrelation* function, we used *runGenie3* function to

580 infer potential transcription factor targets. For building the gene regulatory network, transcriptional

581 factors and their top 10 potential gene targets were predicted with the following SCENIC functions:

582 *runSCENIC_1_coexNetwork2modules*, *runSCENIC_2_createRegulons,* and

583 *runSCENIC_3_scoreCells*. Regulon activity for each cell was calculated as the average

584 normalized expression of putative target genes. Regulon Activity were plotted in a heatmap using

585 the R package ComplexHeatmap (v2.14.0). All required inputs were downloaded from

586 https://resources.aertslab.org/cistarget/databases/old/mus_musculus/mm9/refseq_r45/mc9nr/ge

587 ne_based/.

588

589 **Cynomolgus macaque scRNA-seq analysis**

590 For the cynomolgus macaque granuloma dataset from Bromley *et al.* (*72*), we downloaded the

591 processed scRNA-seq object from the Broad Single Cell Portal. The dataset was filtered to include

592 only CD8$^+$ T cells which are "TEMRA-like," "GZMK^{hi} TEM/PEX-like," "TEff-like," and "Tc17-like"

593 on SubclusteringV2. Primary infection group was selected based on Naïve in the Group_Detailed

594 category. For the cynomolgus macaque granuloma dataset at 10wpi from Gideon *et al.* (*5*), we

595   downloaded raw scRNA-seq data from GSE200151. The dataset was filtered to include only

596   cytotoxic cells ("TCytotoxic1," "TCytotoxic2," "TCytotoxic3," "TCytotoxic4," "TCytotoxic5," and

597   "TCytotoxic6") on SpecificFinal category. *NormalizeData*, *ScaleData*, *FindVariableFeatures*, and

598   *RunPCA* were performed by Seurat (v.4.1.1) with default settings. For the cynomolgus macaque

599   granuloma dataset from Winchell *et al.* (*11*), we downloaded processed scRNA-seq data from the

600   Broad Single Cell Portal. The dataset was filtered to include T/NK cells in the General_Celltypes

601   category, and then CD8$^+$ T cells were further selected based on CD8A > 0.5 AND CD8B > 0.5.

602   Only IgG treated group was used for further analysis. We used 0.5 as a log normalized expression

603   threshold to divide cells into CD226^{hi} (n=609) and CD226^{lo} (n=901) CD8$^+$ T cells. For all datasets,

604   differentially expressed gene analysis was performed between indicated CD8$^+$ T cell populations

605   using the *FindMarkers* function and visualized using EnhancedVolcano (v1.16.0) and ggplot2

606   (v3.5.1). DEGs are listed in Table S6.

607

608   **Human scRNA-seq analysis**

609   scRNA-seq data from resected lungs from active TB patients were downloaded from Wen *et al.*

610   and QC and processed as described earlier in scRNA-seq data processing and analysis. We

611   excluded a sample of SP020L due to the small cell number when integration was performed. The

612   dataset was filtered to only include CD8$^+$ T cells based on CD8A > 0.5 AND CD8B > 0.5 AND

613   CD3E > 1 AND CD4 < 1e-10. We used 0.5 as a log normalized expression threshold to divide

614   cells into CD226^{hi} (n=661) and CD226^{lo} (n=6,580) CD8$^+$ T cells. Differentially expressed gene

615   analysis was performed between CD226^{hi} and CD226^{lo} CD8$^+$ T cells using the *FindMarkers*

616   function and visualized using EnhancedVolcano (v1.16.0) and ggplot2 (v3.5.1). DEGs are listed

617   in Table S6.

618

619   **CD8$^+$ T cell clonotype filtering and analysis**

620   Cell Ranger VDJ pipeline (v6, 10× Genomics) was used to process the raw TCR sequence data

621   with default augments and align them to the mouse reference genome GRCm38 (mm10). CD8$^+$

622   T cells were filtered based on *Cd3e* (>1) AND *Cd8a* AND *Cd8b1* (>0.5) AND *Cd4*< 1e-10 with a

623   single rearranged TCR comprised of a single TCRα and TCRβ chain. CD8$^+$ T cells that met these

624   criteria were then assigned to a clonotype using the nucleotide sequences of the CDR3 region of

625   TCR α and β. Repertoire overlap analysis was performed using R package Immunarch (v1.0.0),

626   using *repOverlap* function with .method = "morisita" and .col = "nt". Because of the large

627   imbalance of cell number in each Seurat cluster, we uniformly down-sampled all clusters to 209

628   cells for clonal overlap calculation. TRV and TRJ repertoires and CDR3 sequences for all TCR

629   clonotypes are listed in Table S2.

630

631   **RNA Sequencing and data analysis**

632   CD226$^+$ or CD226$^-$ CD45-IV$^-$CD44$^+$CD8$^+$ T cells were isolated by flow sorting from 3 C57BL/6J

633   mice each, which were infected with Mtb for 24-28 weeks prior to the sort. Total RNA was

634   extracted from sorted cells stored in RNAprotect (QIAGEN) using Direct-zol RNA Microprep kit

635   (Zymo research) according to the manufacturer's instructions. RNA sequencing with poly(A)

636   selection was performed at GENEWIZ/AZENTA. Sequence reads were trimmed to remove

637   possible adapter sequences and nucleotides with poor quality using fastp v.0.23.1. UMI-based

638   de-duplication was performed using fastp (v.0.23.1) simultaneously. Trimmed and de-duplicated

639   reads were then mapped to the Mus musculus GRCm38 reference genome available on

640   ENSEMBL using the STAR aligner (v.2.5.2b). Normalization and differential gene expression

641   analysis were performed using DESeq2 R package (v1.38.3). The raw read matrix was log2

642   transformed using the *rlogTransformation* function, and Principal component analysis (PCA) was

643   created. For GSEA, we used fgsea (v1.18.0) with MSigDB (v7.5.1)

644   immunologic.signature_gene_sets (C7).

645

646   **Published RNA-Sequencing and Nanostring data analysis**

647 Normalized gene expression values from published RNA-seq data (*63, 64*) and Nanostring data

648 (*29*) were obtained, and Z-scaled scores were shown in a heatmap using the R package

649 pheatmap (v1.0.12).

650

Intracellular cytokine staining

652 Cells were incubated in complete RPMI at 37°C/5% CO2 for 17 hours in the presence or absence

653 of stimulation. In some experiments cells were stimulated with anti-CD3 (1 µg/ml) and anti-CD28

654 (5 µg/ml) for 5 hours. During the last 5 hours of incubation, we added Brefeldin A (eBioscience)

655 at final concentration of 3 ug/ml. Cells were stained with Zombie Fixable Viability dye (Biolegend)

656 and surface staining was performed as described above. Cells were then fixed and permeabilized

657 for 20 minutes at 4°C using BD Cytofix/Cytoperm permeabilization kit (BD Biosciences). Cells

658 were then washed with Perm/Wash buffer and stained with the intracellular antibodies in

659 Perm/Wash buffer for 30 minutes at 4°C. After washing with autoMACS running buffer, stained

660 cells were fixed in 1% paraformaldehyde. Data was collected on a Cytek Aurora (Cytek).

661 Polyfunctionality pie charts were created using SPICE 6.1 provided by the National Institute of

662 Allergy and Infectious Diseases (NIAID).

663

Transcription factor staining

665 Cells were stained with Zombie Fixable Viability dye (Biolegend) and surface staining was

666 performed as described above. Cells were then fixed and permeabilized with the

667 FoxP3/transcription factor buffer staining set (eBioscience) for 20 minutes at RT. Cells were

668 washed with 1X Permeabilization Buffer and stained with antibody cocktail diluted in 1X

669 Permeabilization Buffer for 30 minutes at RT. After washing with autoMACS running buffer,

670 stained cells were fixed in 1% paraformaldehyde. Samples were assessed on a Cytek Aurora

671 (Cytek).

672

Preparation of Mtb

Mtb was grown in 7H9 media (supplemented with 10% OADC, 0.05% of Tween-80, and 0.2% glycerol) until an OD_{600} = 0.6-0.8. The bacteria were washed with RPMI 1640, and incubated with TB coat (RPMI 1640 containing 1% heat-inactivated FBS, 2% human serum, and 0.05% Tween-80) at RT for 5 minutes. After washing again with RPMI 1640, the bacteria passed through a 5 μm filter to remove clumps. OD_{600} was measured again to adjust the concentration with a conversion factor of OD_{600} 1 = 3 $\times$ 10^8 bacteria/ml, providing a multiplicity of infection (MOI) of 0.3, 1, 3 in cRPMI (without antibiotics).

Collecting of thioglycolate-elicited peritoneal macrophages (TG-PMs) and in vitro infection

Thioglycolate was injected into the peritoneal cavity in C57BL/6J or BALB/c mice. After 4 days, peritoneal lavage was collected from peritoneal cavity, and macrophages were purified using CD11b microbeads (Miltenyi). Purified TG-PMs were plated 10^5/well in 96 well flat plates and, once adhered, infected with Mtb overnight at 37°C/5% CO2. TG-PMs infected at MOI 1 were lysed with 1% Triton X-100 the next day (Day 1) and plated with serial dilutions of the lysate on 7H11 plates (Hardy Diagnosis). The plates were incubated for 21 days at 37°C/5% CO2 for Day 1 CFU enumeration.

In vitro coculture of sorted CD8$^+$ T cells and infected TG-PMs

TG-PMs were infected in vitro overnight or left uninfected as described above. The next day, the TG-PMs were washed three times with RPMI1640 to remove any extracellular bacteria. Sorted CD226$^+$ or CD226$^-$ CD45-IV$^-$CD44$^+$CD8$^+$ T cells were added to the TG-PMs at a ratio of 1:2 (T cell to macrophage). The cells were cultured in cRPMI (without antibiotics) at 37°C/5% CO2 for 17 hours in the presence or absence of 25 μg/ml anti-CD226 mAb (10E5, eBioscience). Intracellular cytokine staining was performed as described above.

698

Cytokine measurements in coculture supernatant

Single cell suspensions were prepared from the lungs of Mtb-infected C57BL/6J mice as described above using GentleMACS tissue dissociators (Miltenyi). Cell suspensions were filtered through 70-μm strainers, and red blood cells were lysed in ACK Lysis Buffer (Gibco; Thermo Fisher Scientific). Cell suspensions were then filtered through 40-μm strainers. CD8$^+$ T cells were purified from suspensions using mouse CD8 (TIL) MicroBeads (Miltenyi), resulting in highly pure products (>92% CD8$^+$). Purified CD8$^+$ T cells were cocultured with Mtb-infected TG-PMs (MOI=1) in the presence of anti-CD226 (10E5) or isotype control mAb, both at 25 μg/ml, for 72 hours in cRPMI (without antibiotics) at 37°C/5% CO2. Cell culture supernatant was collected, and mouse Granzyme B was quantified via ELISA (Mouse Granzyme B DuoSet ELISA, R&D Systems) following manufacturer's instructions.

Statistical analysis

Statistical analyses were performed using GraphPad Prism (v10) software. The statistical tests performed for each experiment are specified in the figure legends.

Data availability

Sequencing data generated for this study have been deposited in the Gene Expression Omnibus database with accession code GSE266006.

References

1. R. M. Houben, P. J. Dodd, The Global Burden of Latent Tuberculosis Infection: A Re-estimation Using Mathematical Modelling. *PLoS Med* **13**, e1002152 (2016).

2. C. K. Kwan, J. D. Ernst, HIV and tuberculosis: a deadly human syndemic. *Clin Microbiol Rev* **24**, 351-376 (2011).

3. P. L. Lin *et al.*, CD4 T cell depletion exacerbates acute Mycobacterium tuberculosis while reactivation of latent infection is dependent on severity of tissue depletion in cynomolgus macaques. *AIDS Res Hum Retroviruses* **28**, 1693-1702 (2012).

4. T. Mogues, M. E. Goodrich, L. Ryan, R. LaCourse, R. J. North, The relative importance of T cell subsets in immunity and immunopathology of airborne Mycobacterium tuberculosis infection in mice. *J Exp Med* **193**, 271-280 (2001).

5. H. P. Gideon *et al.*, Multimodal profiling of lung granulomas in macaques reveals cellular correlates of tuberculosis control. *Immunity* **55**, 827-846 e810 (2022).

6. C. Y. Chen *et al.*, A critical role for CD8 T cells in a nonhuman primate model of tuberculosis. *PLoS Pathog* **5**, e1000392 (2009).

7. S. J. Balin *et al.*, Human antimicrobial cytotoxic T lymphocytes, defined by NK receptors and antimicrobial proteins, kill intracellular bacteria. *Sci Immunol* **3**, (2018).

8. M. Busch *et al.*, Lipoarabinomannan-Responsive Polycytotoxic T Cells Are Associated with Protection in Human Tuberculosis. *Am J Respir Crit Care Med* **194**, 345-355 (2016).

9. H. Bruns *et al.*, Anti-TNF immunotherapy reduces CD8+ T cell-mediated antimicrobial activity against Mycobacterium tuberculosis in humans. *J Clin Invest* **119**, 1167-1177 (2009).

10. S. Stenger *et al.*, An antimicrobial activity of cytolytic T cells mediated by granulysin. *Science* **282**, 121-125 (1998).

11. C. G. Winchell *et al.*, CD8+ lymphocytes are critical for early control of tuberculosis in macaques. *J Exp Med* **220**, (2023).

12. S. M. Behar, C. C. Dascher, M. J. Grusby, C. R. Wang, M. B. Brenner, Susceptibility of mice deficient in CD1D or TAP1 to infection with Mycobacterium tuberculosis. *J Exp Med* **189**, 1973-1980 (1999).

13. J. S. Woodworth, Y. Wu, S. M. Behar, Mycobacterium tuberculosis-specific CD8+ T cells require perforin to kill target cells and provide protection in vivo. *J Immunol* **181**, 8595-8603 (2008).

14. S. Stenger *et al.*, Differential effects of cytolytic T cell subsets on intracellular infection. *Science* **276**, 1684-1687 (1997).

15. S. Thoma-Uszynski, S. Stenger, R. L. Modlin, CTL-mediated killing of intracellular Mycobacterium tuberculosis is independent of target cell nuclear apoptosis. *J Immunol* **165**, 5773-5779 (2000).

16. L. A. van Pinxteren, J. P. Cassidy, B. H. Smedegaard, E. M. Agger, P. Andersen, Control of latent Mycobacterium tuberculosis infection is dependent on CD8 T cells. *European Journal of Immunology* **30**, 3689-3698 (2000).

17. Y. J. Lu *et al.*, CD4 T cell help prevents CD8 T cell exhaustion and promotes control of Mycobacterium tuberculosis infection. *Cell Rep* **36**, 109696 (2021).

18. Y. Wu, J. S. Woodworth, D. S. Shin, S. Morris, S. M. Behar, Vaccine-elicited 10-kilodalton culture filtrate protein-specific CD8+ T cells are sufficient to mediate protection against Mycobacterium tuberculosis infection. *Infect Immun* **76**, 2249-2255 (2008).

19. J. Mu *et al.*, Respiratory mucosal immunization with adenovirus gene transfer vector induces helper CD4 T cell-independent protective immunity. *The Journal of Gene Medicine* **12**, 693-704 (2010).

20. J. L. Flynn, M. M. Goldstein, K. J. Triebold, B. Koller, B. R. Bloom, Major histocompatibility complex class I-restricted T cells are required for resistance to

770   Mycobacterium tuberculosis infection. *Proc Natl Acad Sci U S A* **89**, 12013-12017
771   (1992).

772 21.   R. Sutiwisesak *et al.*, A natural polymorphism of Mycobacterium tuberculosis in the esxH
773   gene disrupts immunodomination by the TB10.4-specific CD8 T cell response. *PLoS*
774   *Pathog* **16**, e1009000 (2020).

775 22.   J. D. Yang *et al.*, Mycobacterium tuberculosis-specific CD4+ and CD8+ T cells differ in
776   their capacity to recognize infected macrophages. *PLoS Pathog* **14**, e1007060 (2018).

777 23.   D. Mott *et al.*, High Bacillary Burden and the ESX-1 Type VII Secretion System Promote
778   MHC Class I Presentation by Mycobacterium tuberculosis-Infected Macrophages to CD8
779   T Cells. *J Immunol* **210**, 1531-1542 (2023).

780 24.   Y. R. Patankar *et al.*, Limited recognition of Mycobacterium tuberculosis-infected
781   macrophages by polyclonal CD4 and CD8 T cells from the lungs of infected mice.
782   *Mucosal Immunol* **13**, 140-148 (2020).

783 25.   P. Thakur, R. Sutiwisesak, Y. J. Lu, S. M. Behar, Use of the Human Granulysin
784   Transgenic Mice To Evaluate the Role of Granulysin Expression by CD8 T Cells in
785   Immunity To Mycobacterium tuberculosis. *mBio* **13**, e0302022 (2022).

786 26.   A. J. Zajac *et al.*, Viral immune evasion due to persistence of activated T cells without
787   effector function. *J Exp Med* **188**, 2205-2213 (1998).

788 27.   L. M. McLane, M. S. Abdel-Hakeem, E. J. Wherry, CD8 T Cell Exhaustion During
789   Chronic Viral Infection and Cancer. *Annu Rev Immunol* **37**, 457-495 (2019).

790 28.   M. G. Booty *et al.*, IL-21 signaling is essential for optimal host resistance against
791   Mycobacterium tuberculosis infection. *Sci Rep* **6**, 36720 (2016).

792 29.   P. Jayaraman *et al.*, TIM3 Mediates T Cell Exhaustion during Mycobacterium
793   tuberculosis Infection. *PLoS Pathog* **12**, e1005490 (2016).

794 30.   Z. Wen *et al.*, Integrated single-cell transcriptome and T cell receptor profiling reveals
795   defects of T cell exhaustion in pulmonary tuberculosis. *Journal of Infection* **88**, (2024).

796 31.   J. Pan *et al.*, Landscape of Exhausted T Cells in Tuberculosis Revealed by Single-Cell
797   Sequencing. *Microbiol Spectr* **11**, e0283922 (2023).

798 32.   E. A. Wong *et al.*, Low Levels of T Cell Exhaustion in Tuberculous Lung Granulomas.
799   *Infect Immun* **86**, (2018).

800 33.   A. Shibuya *et al.*, DNAM-1, a novel adhesion molecule involved in the cytolytic function
801   of T lymphocytes. *Immunity* **4**, 573-581 (1996).

802 34.   H. Huang *et al.*, CD226 identifies functional CD8(+)T cells in the tumor
803   microenvironment and predicts a better outcome for human gastric cancer. *Front*
804   *Immunol* **14**, 1150803 (2023).

805 35.   M. Braun *et al.*, CD155 on Tumor Cells Drives Resistance to Immunotherapy by
806   Inducing the Degradation of the Activating Receptor CD226 in CD8(+) T Cells. *Immunity*
807   **53**, 805-823 e815 (2020).

808 36.   H. S. Jin *et al.*, CD226(hi)CD8(+) T Cells Are a Prerequisite for Anti-TIGIT
809   Immunotherapy. *Cancer Immunol Res* **8**, 912-925 (2020).

810 37.   M. Weulersse *et al.*, Eomes-Dependent Loss of the Co-activating Receptor CD226
811   Restrains CD8(+) T Cell Anti-tumor Functions and Limits the Efficacy of Cancer
812   Immunotherapy. *Immunity* **53**, 824-839 e810 (2020).

813 38.   T. Sundell *et al.*, Single-cell RNA sequencing analyses: interference by the genes that
814   encode the B-cell and T-cell receptors. *Brief Funct Genomics* **22**, 263-273 (2022).

815 39.   B. C. Miller *et al.*, Subsets of exhausted CD8(+) T cells differentially mediate tumor
816   control and respond to checkpoint blockade. *Nat Immunol* **20**, 326-336 (2019).

817 40.   J. T. Ingram, J. S. Yi, A. J. Zajac, Exhausted CD8 T cells downregulate the IL-18
818   receptor and become unresponsive to inflammatory cytokines and bacterial co-
819   infections. *PLoS Pathog* **7**, e1002273 (2011).

41. S. Yenyuwadee, J. L. Sanchez-Trincado Lopez, R. Shah, P. C. Rosato, V. A. Boussiotis, The evolving role of tissue-resident memory T cells in infections and cancer. *Sci Adv* **8**, eabo5871 (2022).

42. A. P. Nath *et al.*, Comparative analysis reveals a role for TGF-beta in shaping the residency-related transcriptional signature in tissue-resident memory CD8+ T cells. *PLoS One* **14**, e0210495 (2019).

43. K. A. Casey *et al.*, Antigen-independent differentiation and maintenance of effector-like resident memory T cells in tissues. *J Immunol* **188**, 4866-4875 (2012).

44. L. K. Mackay *et al.*, The developmental pathway for CD103(+)CD8+ tissue-resident memory T cells of skin. *Nat Immunol* **14**, 1294-1301 (2013).

45. B. S. Sheridan *et al.*, Oral infection drives a distinct population of intestinal resident memory CD8(+) T cells with enhanced protective function. *Immunity* **40**, 747-757 (2014).

46. N. Zhang, M. J. Bevan, Transforming growth factor-beta signaling controls the formation and maintenance of gut-resident memory T cells by regulating migration and retention. *Immunity* **39**, 687-696 (2013).

47. T. Hirai *et al.*, Competition for Active TGFbeta Cytokine Allows for Selective Retention of Antigen-Specific Tissue- Resident Memory T Cells in the Epidermal Niche. *Immunity* **54**, 84-98 e85 (2021).

48. S. S. Gabriel *et al.*, Transforming growth factor-beta-regulated mTOR activity preserves cellular metabolism to maintain long-term T cell responses in chronic infection. *Immunity* **54**, 1698-1714 e1695 (2021).

49. Z. A. Clarke, G. D. Bader, MALAT1 expression indicates cell quality in single-cell RNA sequencing data. *bioRxiv*, 2024.2007.2014.603469 (2024).

50. N. Weisshaar *et al.*, Rgs16 promotes antitumor CD8(+) T cell exhaustion. *Sci Immunol* **7**, eabh1873 (2022).

51. S. Aibar *et al.*, SCENIC: single-cell regulatory network inference and clustering. *Nat Methods* **14**, 1083-1086 (2017).

52. J. Li, Y. He, J. Hao, L. Ni, C. Dong, High Levels of Eomes Promote Exhaustion of Anti-tumor CD8(+) T Cells. *Front Immunol* **9**, 2981 (2018).

53. P. Jiang *et al.*, Systematic investigation of cytokine signaling activity at the tissue and single-cell levels. *Nat Methods* **18**, 1181-1191 (2021).

54. N. Chihara *et al.*, Induction and transcriptional regulation of the co-inhibitory gene module in T cells. *Nature* **558**, 454-459 (2018).

55. M. Y. Kasmani *et al.*, Clonal lineage tracing reveals mechanisms skewing CD8+ T cell fate decisions in chronic infection. *J Exp Med* **220**, (2023).

56. S. Lukhele *et al.*, The transcription factor IRF2 drives interferon-mediated CD8(+) T cell exhaustion to restrict anti-tumor immunity. *Immunity* **55**, 2369-2385 e2310 (2022).

57. M. Andreatta *et al.*, Interpretation of T cell states from single-cell transcriptomics data using reference atlases. *Nat Commun* **12**, 2965 (2021).

58. J. R. Giles *et al.*, Shared and distinct biological circuits in effector, memory and exhausted CD8(+) T cells revealed by temporal single-cell transcriptomics and epigenetics. *Nat Immunol* **23**, 1600-1613 (2022).

59. C. Trapnell *et al.*, The dynamics and regulators of cell fate decisions are revealed by pseudotemporal ordering of single cells. *Nat Biotechnol* **32**, 381-386 (2014).

60. J. Cao *et al.*, The single-cell transcriptional landscape of mammalian organogenesis. *Nature* **566**, 496-502 (2019).

61. Z. Chen *et al.*, TCF-1-Centered Transcriptional Network Drives an Effector versus Exhausted CD8 T Cell-Fate Decision. *Immunity* **51**, 840-855 e845 (2019).

62. D. T. Utzschneider *et al.*, Early precursor T cells establish and propagate T cell exhaustion in chronic infection. *Nat Immunol* **21**, 1256-1266 (2020).

63. W. H. Hudson *et al.*, Proliferating Transitory T Cells with an Effector-like Transcriptional Signature Emerge from PD-1(+) Stem-like CD8(+) T Cells during Chronic Infection. *Immunity* **51**, 1043-1058 e1044 (2019).

64. M. Singer *et al.*, A Distinct Gene Module for Dysfunction Uncoupled from Activation in Tumor-Infiltrating T Cells. *Cell* **166**, 1500-1511 e1509 (2016).

65. H. T. Jin *et al.*, Cooperation of Tim-3 and PD-1 in CD8 T-cell exhaustion during chronic viral infection. *Proc Natl Acad Sci U S A* **107**, 14733-14738 (2010).

66. R. L. Reinhardt, H. E. Liang, R. M. Locksley, Cytokine-secreting follicular T cells shape the antibody repertoire. *Nat Immunol* **10**, 385-393 (2009).

67. R. L. Reinhardt *et al.*, A novel model for IFN-gamma-mediated autoinflammatory syndromes. *J Immunol* **194**, 2358-2368 (2015).

68. R. Lai *et al.*, Host genetic background is a barrier to broadly effective vaccine-mediated protection against tuberculosis. *J Clin Invest* **133**, (2023).

69. K. Shibuya *et al.*, CD226 (DNAM-1) is involved in lymphocyte function-associated antigen 1 costimulatory signal for naive T cell differentiation and proliferation. *J Exp Med* **198**, 1829-1839 (2003).

70. S. Gilfillan *et al.*, DNAM-1 promotes activation of cytotoxic lymphocytes by nonprofessional antigen-presenting cells and tumors. *J Exp Med* **205**, 2965-2973 (2008).

71. C. Bottino *et al.*, Identification of PVR (CD155) and Nectin-2 (CD112) as cell surface ligands for the human DNAM-1 (CD226) activating molecule. *J Exp Med* **198**, 557-567 (2003).

72. J. D. Bromley *et al.*, CD4(+) T cells re-wire granuloma cellularity and regulatory networks to promote immunomodulation following Mtb reinfection. *Immunity*, (2024).

73. Z. Wen *et al.*, Integrated single-cell transcriptome and T cell receptor profiling reveals defects of T cell exhaustion in pulmonary tuberculosis. *J Infect* **88**, 106158 (2024).

74. G. F. Burns, T. Triglia, J. A. Werkmeister, C. G. Begley, A. W. Boyd, TLiSA1, a human T lineage-specific activation antigen involved in the differentiation of cytotoxic T lymphocytes and anomalous killer cells from their precursors. *J Exp Med* **161**, 1063-1078 (1985).

75. K. L. Banta *et al.*, Mechanistic convergence of the TIGIT and PD-1 inhibitory pathways necessitates co-blockade to optimize anti-tumor CD8(+) T cell responses. *Immunity* **55**, 512-526 e519 (2022).

76. K. D. Kauffman *et al.*, PD-1 blockade exacerbates Mycobacterium tuberculosis infection in rhesus macaques. *Sci Immunol* **6**, (2021).

77. Y. Qiu *et al.*, Tim-3-expressing CD4+ and CD8+ T cells in human tuberculosis (TB) exhibit polarized effector memory phenotypes and stronger anti-TB effector functions. *PLoS Pathog* **8**, e1002984 (2012).

78. J. V. Gorman *et al.*, Tim-3 directly enhances CD8 T cell responses to acute Listeria monocytogenes infection. *J Immunol* **192**, 3133-3142 (2014).

79. J. Lee *et al.*, Phosphotyrosine-dependent coupling of Tim-3 to T-cell receptor signaling pathways. *Mol Cell Biol* **31**, 3963-3974 (2011).

80. L. Avery, J. Filderman, A. L. Szymczak-Workman, L. P. Kane, Tim-3 co-stimulation promotes short-lived effector T cells, restricts memory precursors, and is dispensable for T cell exhaustion. *Proc Natl Acad Sci U S A* **115**, 2455-2460 (2018).

81. S. Kataoka *et al.*, The costimulatory activity of Tim-3 requires Akt and MAPK signaling and its recruitment to the immune synapse. *Sci Signal* **14**, (2021).

82. J. Fourcade *et al.*, Upregulation of Tim-3 and PD-1 expression is associated with tumor antigen-specific CD8+ T cell dysfunction in melanoma patients. *J Exp Med* **207**, 2175-2186 (2010).

83. C. N. Ratnatunga *et al.*, Characterizing and correcting immune dysfunction in non-tuberculous mycobacterial disease. *Front Immunol* **13**, 1047781 (2022).

84. R. B. Jones *et al.*, Tim-3 expression defines a novel population of dysfunctional T cells with highly elevated frequencies in progressive HIV-1 infection. *J Exp Med* **205**, 2763-2779 (2008).

85. L. Golden-Mason *et al.*, Negative immune regulator Tim-3 is overexpressed on T cells in hepatitis C virus infection and its blockade rescues dysfunctional CD4+ and CD8+ T cells. *J Virol* **83**, 9122-9130 (2009).

86. Y. Cai *et al.*, Single-cell immune profiling reveals functional diversity of T cells in tuberculous pleural effusion. *J Exp Med* **219**, (2022).

87. Y. Li *et al.*, CD226 as a genetic adjuvant to enhance immune efficacy induced by Ag85A DNA vaccination. *Int Immunopharmacol* **25**, 10-18 (2015).

88. A. A. Chackerian, T. V. Perera, S. M. Behar, Gamma interferon-producing CD4+ T lymphocytes in the lung correlate with resistance to infection with Mycobacterium tuberculosis. *Infect Immun* **69**, 2666-2674 (2001).

89. J. Lee *et al.*, CD11cHi monocyte-derived macrophages are a major cellular compartment infected by Mycobacterium tuberculosis. *PLoS Pathog* **16**, e1008621 (2020).

945 **Author contributions:**

946 Conceptualization: TS, SMB

947 Investigation: TS, EC, KC, RL, TR

948 Formal analysis: TS, RL, SMB

949 Writing & Editing: TS, SMB, RL, TR

950 Supervision: SMB

951 Funding Acquisition: SMB

952

953 **Competing interests:** Authors declare that they have no competing interests.
954

955 **Data and materials availability:** Sequencing data generated for this study have been deposited

956 in the Gene Expression Omnibus database with accession code GSE266006. All other data are

957 available in the main text or the supplementary materials.

958

Supplementary Materials:

Supplemental Figure 1. Nine distinct lung parenchymal CD8$^+$ T cell transcriptional states are identified during Mtb infection.

Supplemental Figure 2. Transcriptional analysis of CD226$^+$CD8$^+$ T cells demonstrates expression of an effector program.

Supplemental Figure 3. CD226 expression on lung immune cell subsets.

Supplemental Figure 4. IFNγ-eYFP expression correlates with intracellular IFNγ measured by ICS on T cells from IFNγ-eYFP mice.

Supplemental Figure 5. CD226 expression identifies terminally differentiated effector CD8$^+$ T cells.

Supplemental Figure 6. Representative gating strategies for myeloid cells and T cells.

Table S1. DEGs expressed by each cluster in scRNA-seq of lung parenchymal CD8$^+$ T cells from 6 and 41wpi. 3 tabs corresponds top 30 upregulated genes (tab1), DEGs with average log2 fold change >0.5 or <-0.5, and adjusted P value < 0.01 (tab2) and DEGs with average log2 fold change >0.1 or <-0.1 and adjusted P value < 0.01 (tab3) in each cluster.

Table S2. scTCR-Seq of lung parenchymal CD8$^+$ T cells from 6 and 41wpi.

Table S3. DEGs between T$_{EFF/RM}$ branch [T$_{EFF}$/0, T$_{SL-M}$/2, T$_{RM}$/4, and T$_{POLY}$/6] and T$_{EXH}$ branch [T$_{EXH}$/1 and T$_{IFN}$/8] (log2FC > 0.5 or <-0.5, adjusted P value ≤ 0.01), related to Figure 2D.

Table S4. DEGs between lung parenchymal (CD45-IV$^-$) CD226$^+$ and CD226$^-$ CD44$^+$ CD8$^+$ T cells from mice with chronic infection (24-28wpi) analyzed by RNA-Seq, related to Figure 3A, B and Figure S2A.

Table S5. List of modules of coregulated genes identified by Monocle3 in scRNA-seq of lung parenchymal CD8$^+$ T cells from 6 and 41wpi, related to Figure S2B, C. The genes that had a significant q-value (<0.05) from the autocorrelation analysis were grouped into 49 distinct co-regulated modules.

Table S6. DEGs between CD226^{hi} and CD226^{lo} CD8$^+$ T cells in reanalyzed published datasets, related to Figure 7.
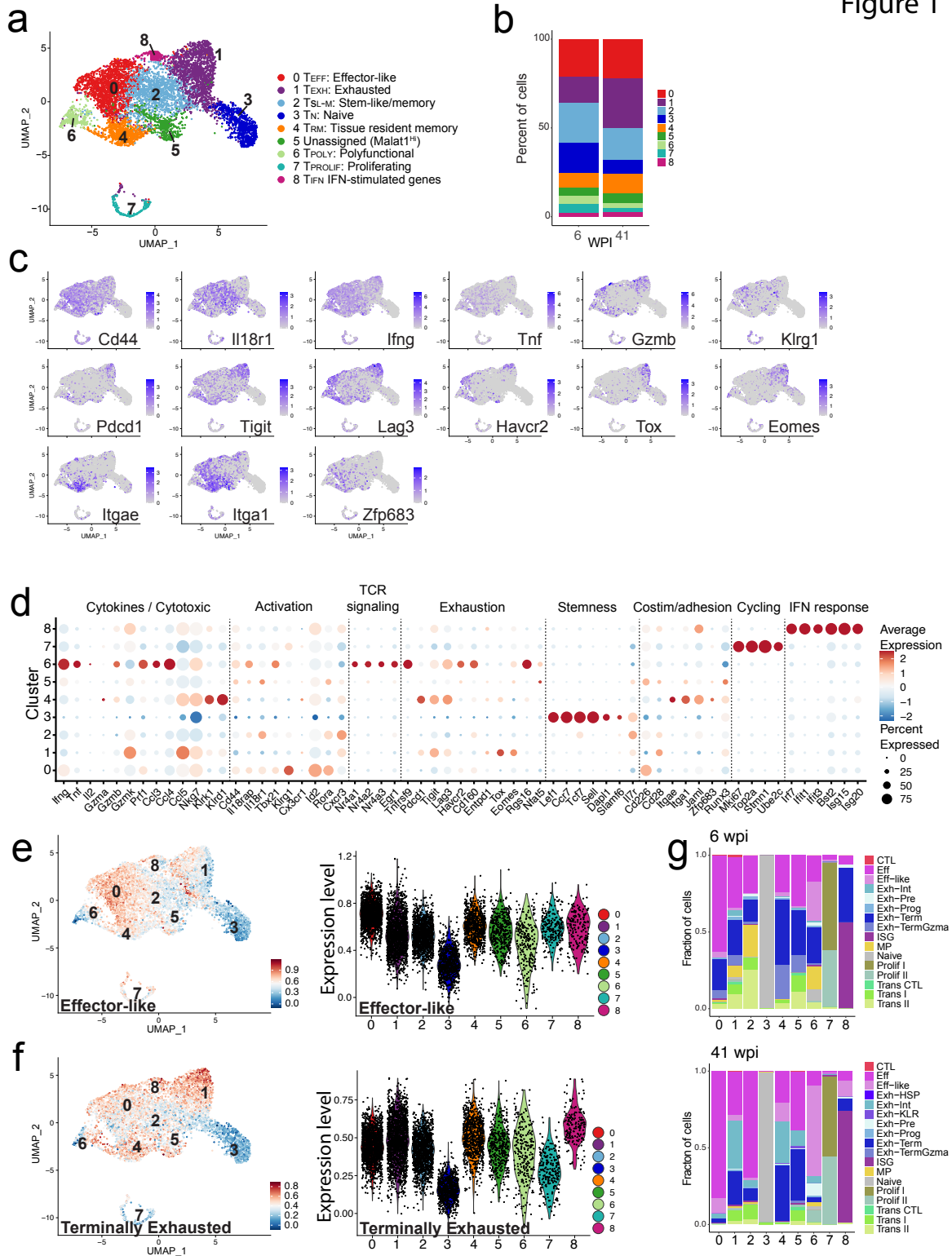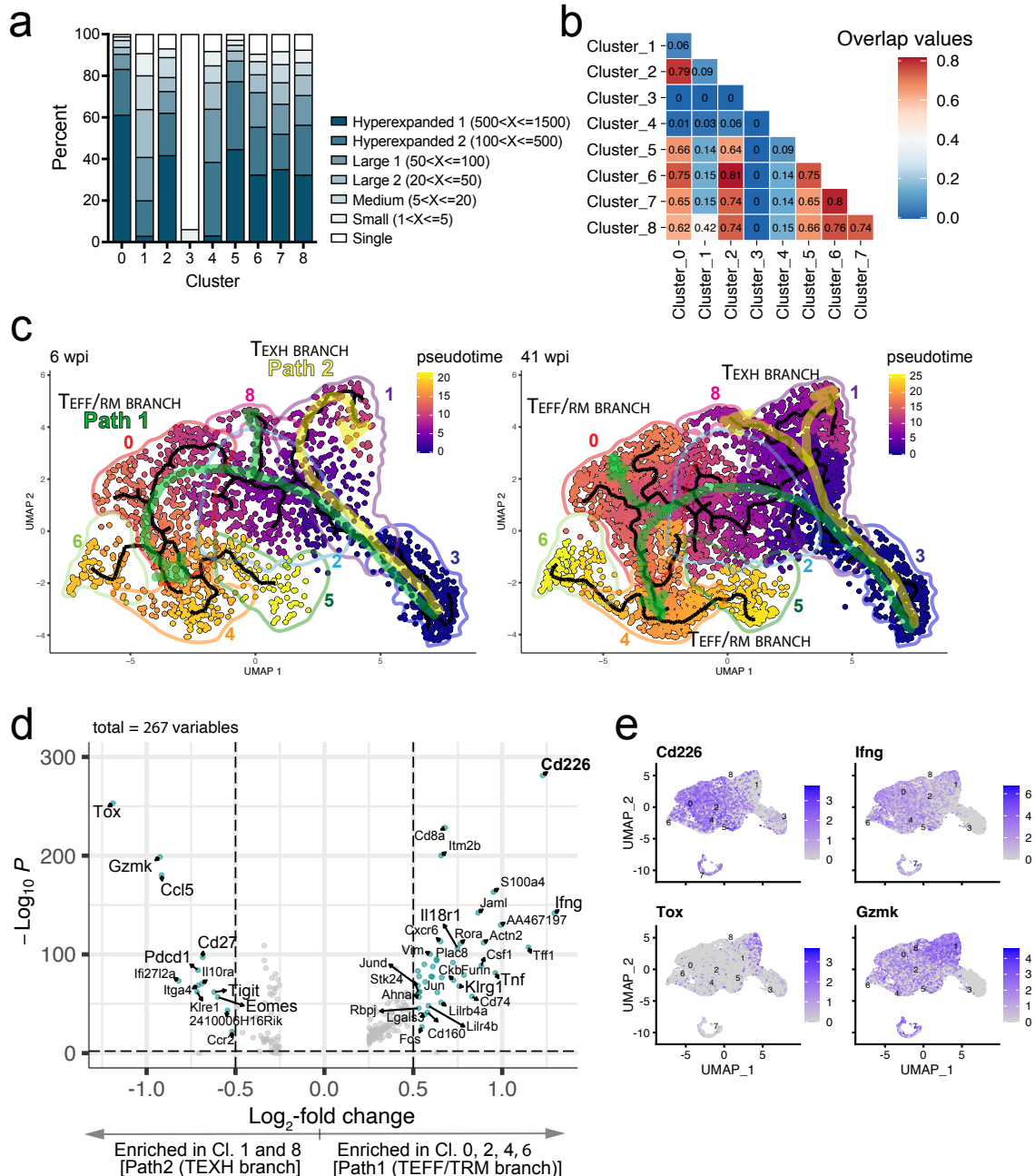
Figure 1. Nine distinct lung parenchymal CD8+ T cell states are identified during Mtb infection. A) UMAP visualization of scRNAseq data of lung parenchymal CD8+ T cells from mice infected with Mtb for 6 and 41 weeks. **B)** Stacked bar graphs depict the cluster distribution at 6 and 41 wpi. **C)** Feature plots of the indicated gene transcripts. **D)** Dot plot of selected function-

1002   associated genes among the CD8$^+$ T cell clusters. **E, F)** UMAP colored based on enrichment of
1003   'effector-like' or 'terminally exhausted' gp33-specific CD8$^+$ T cell signatures from LCMV Clone 13
1004   infection [GSE122712](*39*) and violin plots of the enrichment score. **G)** Transferred cluster
1005   annotations of gp33-specific splenic CD8$^+$ T cells from the combined datasets of LCMV-
1006   Armstrong- and LCMV-Cl13-infected mice [GSE199565](*58*) to our CD8$^+$ T cell clusters at 6 and
1007   41 wpi.
1008
1009

Figure 2. Developmental bifurcation of effector-like/tissue-resident memory and exhausted CD8+ T cells differentiated by *Cd226* expression. A) Stacked bar plots of clonal sizes among clusters. **B)** Plot denoting the Morisita index value for each cluster comparison demonstrating the TCR clonotype overlap. **C)** Single-cell trajectories constructed using Monocle3. UMAP shows cells colored by pseudotime values along the trajectory (black line) at 6 wpi (left) and 41 wpi (right). Cluster number is denoted on the UMAP. T_{PROLIF}/7 is excluded from the analysis. **(D)** Volcano plot of DEGs between T_{EFF}/RM branch [T_{EFF}/0, T_{SL-M}/2, T_{RM}/4, and T_{POLY}/6] and T_{EXH} branch [T_{EXH}/1 and T_{IFN}/8]. Genes with log2FC >0.5 and an adjusted p value < 0.01 are designated by a green filled circle. **(E)** Feature plots of *Cd226*, *Ifng*, *Tox*, and *Gzmk* transcripts.
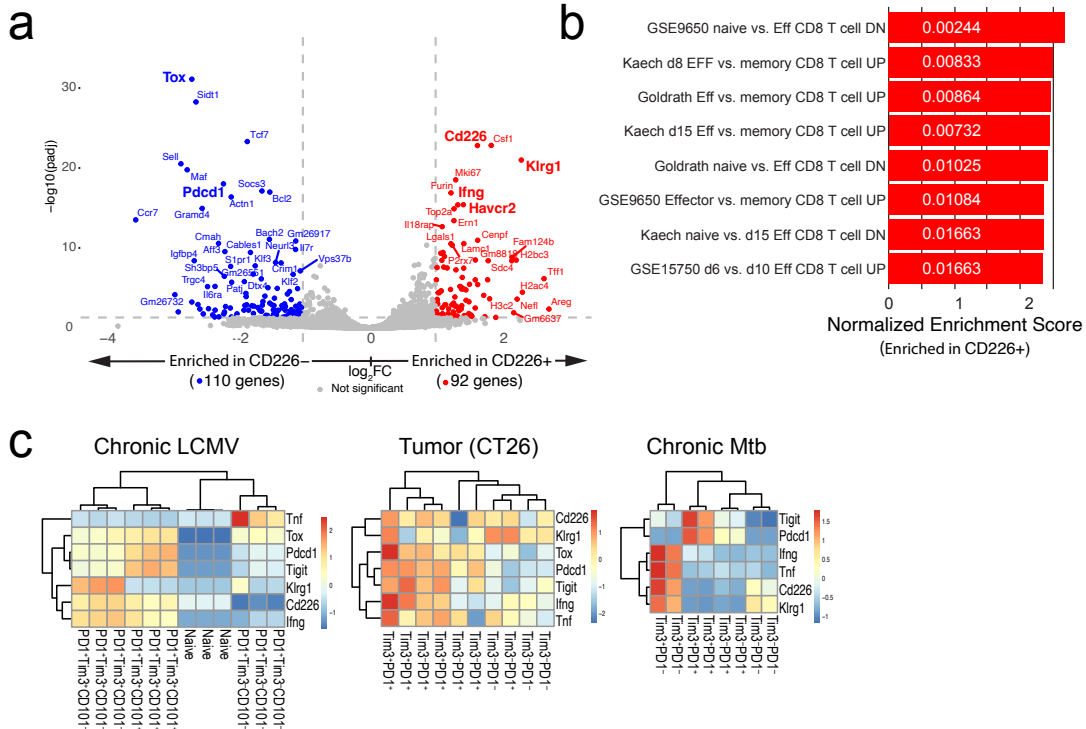
Figure 3. *Cd226* expression identifies CD8+ T cells with effector program during Mtb infection. (A) Volcano plot of DEGs between parenchymal CD226+ and CD226− CD44+CD8+ T cells from the lungs of Mtb-infected mice at 24-28 wpi determined by RNAseq (log2FC>1, adjusted P value ≤ 0.05). **(B)** GSEA of differentially expressed genes in CD226+ CD8+ T cells versus CD226− CD8+ T cells with log2FC>1 and adjusted P value ≤ 0.05 using MSigDB immunologic signature gene sets (C7). Adjusted P values are denoted in the bar. **(C)** Heatmaps of *Cd226*, *Ifng*, *Tnf*, *Pdcd1*, *Tigit*, *Klrg1,* and *Tox* expression (presented as z-score) for indicated CD8+ T cell subsets flow-sorted by PD-1 and TIM-3 (and CD101 in LCMV Clone13) expression determined by RNA-seq for LCMV Clone13(*63*) (left, n=3 donor), CT26 colon carcinoma(*64*) (middle, n=3-4 donor), and TB(*29*) (right, n=2 donor).
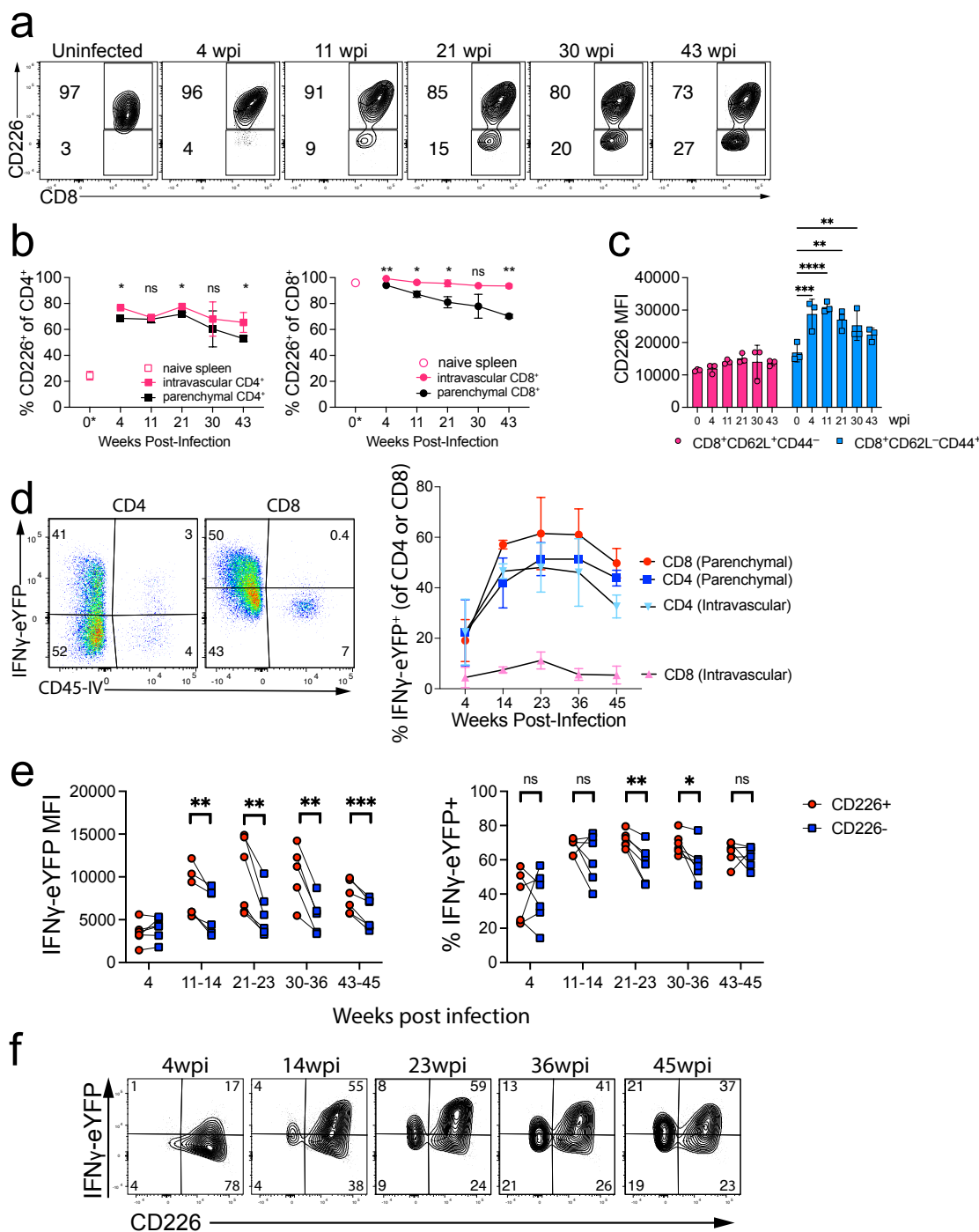
Figure 4. CD226⁺CD8⁺ T cells are activated in vivo during Mtb infection. (**A-C**) CD226 expression by CD8⁺ or CD4⁺ T cells from spleens of uninfected mice or CD8⁺ or CD4⁺ T cells from lungs of Mtb-infected mice was determined by flow cytometry. (**A**) Representative flow cytometry plots. (**B**) Percentage of CD226 expression by naïve splenic T cells from uninfected mice (0 wpi) or lung CD45-IV⁺ or CD45-IV⁻ T cells from Mtb-infected mice. CD4⁺ T cells (left) and CD8⁺ T cells (left) are shown. (**C**) Mean fluorescence intensity (MFI) of CD226 by CD8⁺ T cells from spleens of uninfected mice (0 wpi) or naïve (CD44⁻CD62L⁺) or antigen-experienced (CD44⁺CD62L⁻) lung CD45-IV⁻ CD8⁺ T cells. (**D**) IFNγ-eYFP expression by antigen-experienced (CD44⁺CD62L⁻) CD4⁺ or CD8⁺ T cells by lung CD45-IV⁺ or CD45-IV⁻ from Mtb-infected IFNγ-eYFP reporter mice. Shown

1044   are representative flow cytometry plots at 14 wpi (left) and quantification (right). **(E)** Quantification

1045   of IFNγ-eYFP MFI and percentage of lung antigen-experienced (CD44$^+$CD62L$^-$) CD226$^+$ versus

1046   CD226$^-$ CD8$^+$ T cells from IFNγ-eYFP reporter mice infected with Mtb. **(F)** Representative flow

1047   cytometry plots of CD45-IV$^-$ antigen-experienced (CD44$^+$CD62L$^-$) CD8$^+$ T cells from Mtb-infected

1048   IFNγ-eYFP reporter mice for the indicated duration. **(A-F)** Data from three mice per group,

1049   representative of three experiments. Data is mean ± SEM. Statistical testing was performed using

1050   a paired, two-tailed Student's *t* test (B, E) or a two-way ANOVA (C). *, $p < 0.05$; **, $p < 0.01$; ***,

1051 $p < 0.005$; ****, $p < 0.001$; ns, not significant. Numbers in the drawn gates are percentages.

1052

1053
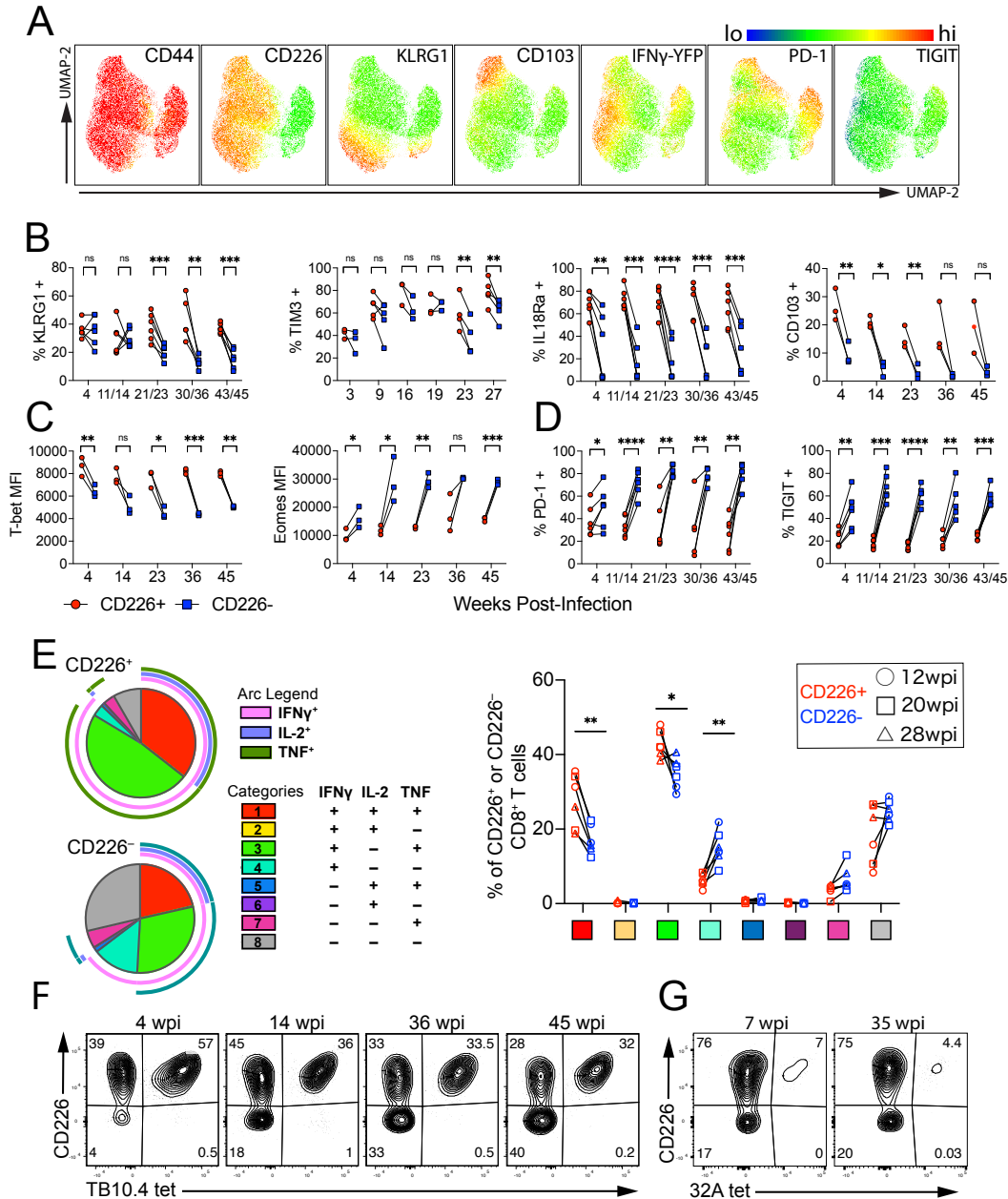
Figure 5. CD226⁺CD8⁺ T cells are terminally differentiated effectors with polyfunctional capacity. (A-D) Flow cytometric analysis of lung antigen-experienced (CD44⁺CD62L⁻) CD45-IV⁻ CD226⁺ and CD226⁻ CD8⁺ T cells from IFNγ-eYFP mice infected with Mtb. **(A)** UMAP visualization of all the antigen-experienced (CD44⁺CD62L⁻) CD45-IV⁻ CD8⁺ T cells from all combined timepoints (4, 14, 23, 36, and 45 wpi) and expression of the indicated markers were overlayed. **(B)** Quantification of the percentage of KLRG1, TIM3, IL18Rα, and CD103 expression. **(C)** Quantification of the MFI of T-bet and Eomes. **(D)** Quantification of the percentage of PD-1 and TIGIT expression. **(E)** Graph depicts the percentage of IFNγ, IL-2, and TNF expressing populations of sorted CD226⁺ and CD226⁻ lung CD45-IV⁻ CD44⁺CD8⁺ T cells stimulated with anti-CD3 and anti-CD28. Representative SPICE graph visualization at 12 wpi (left) and quantification (right). Representative flow cytometry plots of CD226 expression by TB10.4₄₋₁₁-specific **(F)** or 32A₃₀₉₋₃₁₈-specific **(G)** lung CD45-IV⁻ antigen-experienced (CD44⁺CD62L⁻) CD8⁺ T cells from IFNγ-eYFP reporter mice infected with Mtb for indicated weeks. Numbers in the drawn gates are

1068   percentages. Data from three mice per group, representative of 3 (A-D, F, G) or 2 (E) experiments.
1069   Statistical testing was performed using a paired, two-tailed Student's *t* test. *, $p < 0.05$; **, $p <$
1070   0.01; ***, $p < 0.005$; ****, $p < 0.001$; ns, not significant.
1071
1072
1073

Figure 6
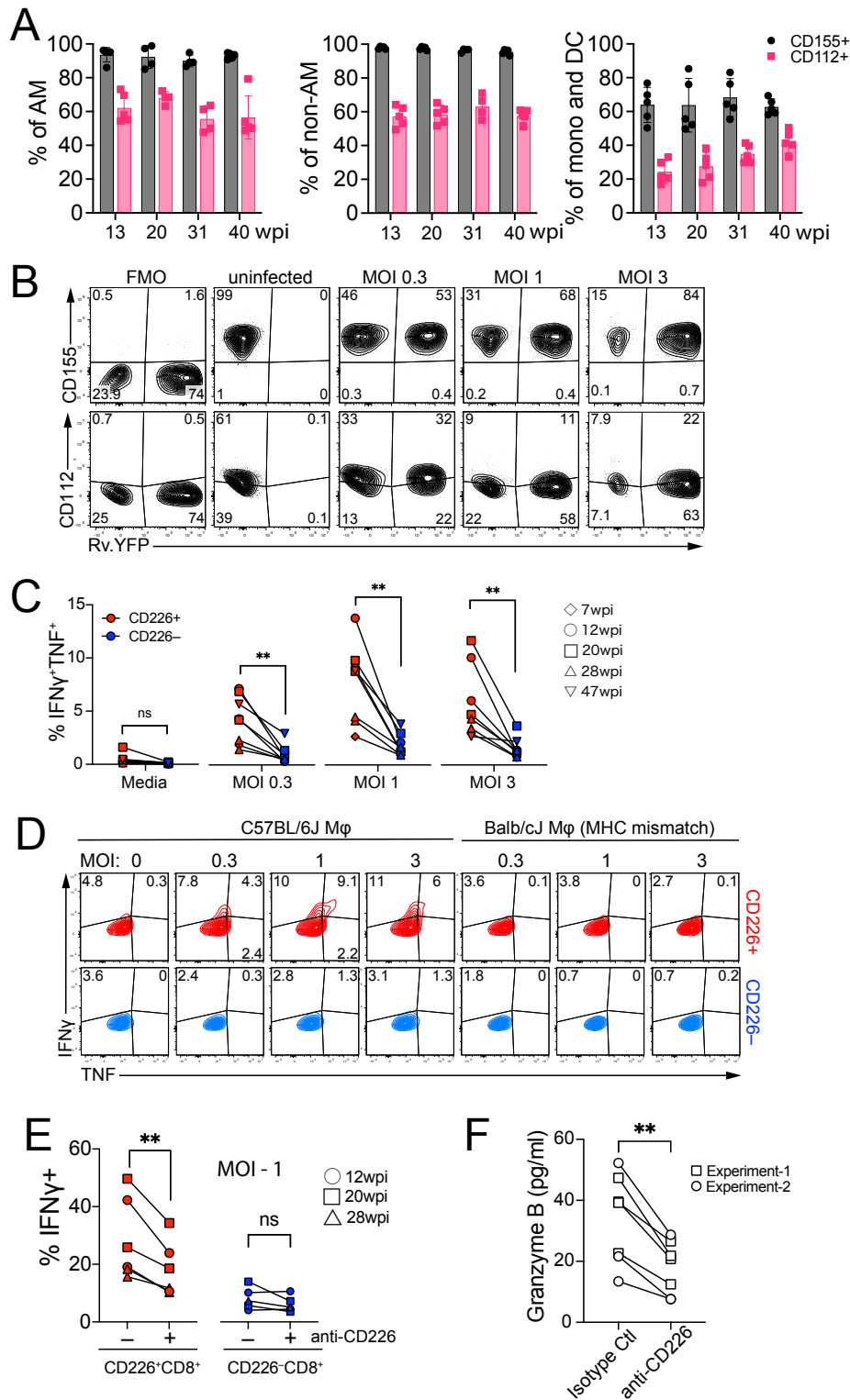
Figure 6. CD226 identifies and costimulates CD8+ T cells that recognize infected macrophages. (A) CD155 (grey) and CD112 (pink) expression by AM, non-AM macrophages (non-AM), monocyte and dendritic cells (mono and DC) from Mtb-infected lungs for indicated weeks. n=4-5. See Fig.S6A for gating strategy. **(B)** Flow cytometry plots showing CD155 or CD112 expression by uninfected, H37Rv-YFP infected or bystander TG-PMs. MOI, multiplicity of

1080 infection (MOI). FMO, fluorescence minus one control. (**C-E**) IFNγ and TNF production by flow-
1081 sorted lung CD45-IV⁻ CD226⁺ or CD226⁻ CD44⁺CD8⁺ T cells cultured with infected TG-PMs at
1082 the indicated MOI for 17 h. TG-PMs are from C57BL/6J (matched) or Balb/cJ (mismatched) mice.
1083 See Fig.S6B for gating strategy. Quantification (**C**) and representative flow cytometry plots of IFNγ
1084 and TNF production by CD8⁺ T cells from mice infected with Mtb for 12 weeks (**D**). **(E)** IFNγ
1085 production by flow-sorted lung CD45-IV⁻ CD226⁺ or CD226⁻ CD44⁺CD8⁺ T cells cultured with
1086 infected TG-PMs at an MOI=1 for 17 hours in the presence or absence of anti-CD226 mAb. **(F)**
1087 Granzyme B secretion by lung CD8⁺ T cells cultured with infected TG-PMs at an MOI=1 for 3 days
1088 in the presence of anti-CD226 or an isotype control mAb. Results are representative of 2-3
1089 experiments (A, B, F) or pooled from 2 experiments (n=8) (C-E). Numbers in the drawn gates are
1090 percentages (B, D). Statistical testing was performed using a paired, two-tailed Student's *t* test
1091 (C, E, F). *, $p < 0.05$; **, $p < 0.01$; ***, $p < 0.001$; ns, not significant.
1092
1093
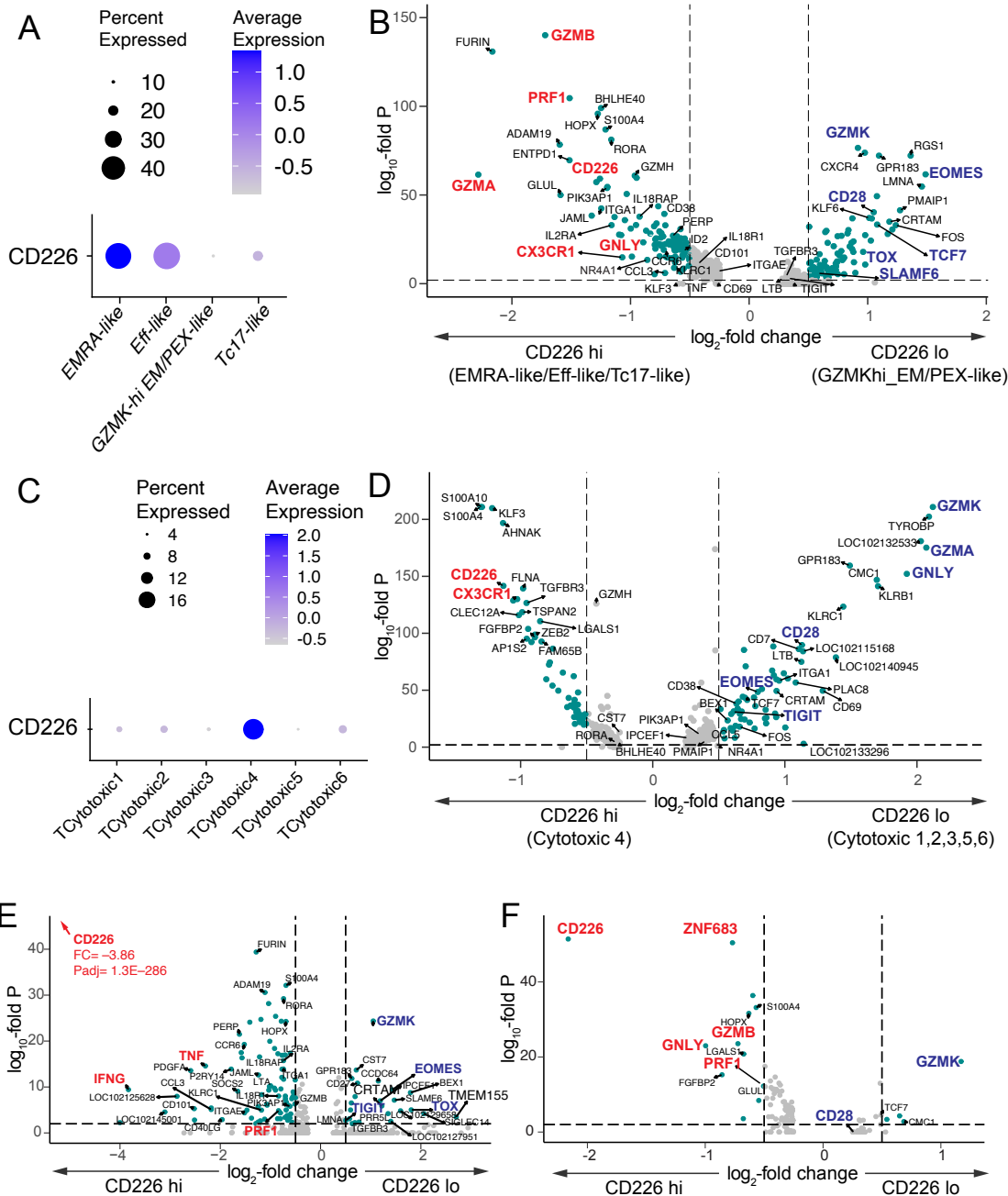
Figure 7. *CD226* and *GZMK* expression identify distinct lung CD8+ T cell subsets in Mtb infected macaque and human. (A) *CD226* expression by lung granuloma CD8+ T cell clusters during primary TB of cynomolgus macaques as defined by Bromley et al. **(B)** Volcano plots of DEGs between *CD226*hi (TEMRA-like, TEFF-like, and Tc17-like) and *CD226*lo (*GZMK*hi TEM/PEX-like) CD8+ T cells during primary TB, based on reanalysis of data from Bromley et al. **(C)** *CD226* expression by lung granuloma cytotoxic cells from infected cynomolgus macaques as defined by Gideon et al. **(D)** Volcano plot of DEGs between *CD226*hi (Cytotoxic 4) and *CD226*lo (Cytotoxic 1,2,3,5,6) cytotoxic cells based on reanalysis of data from Gideon et al. (E) Volcano plot of DEGs between *CD226*hi (log normalized expression>0.5, n=609) and *CD226*lo (log normalized expression<0.5, n=901) of reanalyzed lung granuloma CD8+ T cells in infected cynomolgus macaques from Winchell et al. (*11*). **(F)** Volcano plot of DEGs between CD226hi (log normalized expression>0.5, n=661) and CD226lo (log normalized expression<0.5, n=6,580) of reanalyzed

1107   CD8$^+$ T cells from resected lungs of TB patients described by Wen et al. (*73*) **(B, D, E, F)** Genes
1108   with log2FC >0.5 and an adjusted p value < 0.01 are designated by a green filled circle.
1109